# Chapter 5

# Travel Time Tomography With 3-D Reference Models

In global travel time tomography usually one-dimensional (1-D) reference models are used with respect to which the forward tomographic problem is linearized. This leads to delay times, ray path geometry, earthquake hypocenters and origin times which are computed for the 1-D reference model. The delay time is the basic datum for tomographic inversion in which it is back-projected along reference model ray paths into the 3-D seismic wave speed of the Earth's interior. As a result of insufficient data the tomographic inverse problem is underdetermined which leads to tomographic models biased towards the reference model.
In this study, the dependence of a tomographic model on the reference model is investigated for the particular case of global travel time tomography. For this purpose we perform tomographic analyses with three different reference models, one 1-D model and two 3-D models. The 1-D model (ak135) has been used in various global studies and serves both to provide the link to earlier studies and to provide a comparison to our experiments with 3-D reference models. The first 3-D reference model we use is constructed from recent mantle tomography models which are based on long period seismic data and independent inversion techniques. These models provide a long wavelength background of mantle structure. The second 3-D reference model is an adaptation of the first reference model where we included the detailed structure imaged with short period data in the well resolved parts of the mantle.
Prior to tomographic inversion, earthquakes are relocated in the 3-D reference model using a grid search technique and 3-D ray tracing. This also provides the linearization of the forward problem with respect to the 3-D reference model and results in a delay time data set which is consistent with the reference model.
We observe that in well resolved mantle volumes the imaged structure is independent of the reference model which supports the actual existence of imaged mantle anomalies and gives independent credit to the resolving power of the large set of short period travel time data used. In poorly resolved regions the different tomographic models prove to be reference model dependent. An important outcome of our experiments is a new tomographic model that combines in a consistent way the structure imaged with short period travel times with the

structure imaged with long period data (long period S wave data, surface waves and normal modes). This model is specifically useful, for example, for applications in forward modeling of seismic wave propagation, regional and global event location, mantle dynamics studies and analysis of the Earth's gravity field.

## 5.1 Introduction

Global travel time tomography is a well established and powerful tool to image the seismic velocity properties of the Earth's crust and mantle in detail. To retain computational feasibility and reduce mathematical complexity, simplifications are made in the process of creating a tomographic model. Regarding mathematical complexity, seismic tomography is a nonlinear inverse problem as a result of the dependence of ray geometry (or Fresnel zone in finite-frequency tomography) on the seismic wave speed and of seismic travel times on earthquake location. The forward problem is, however, always linearized with respect to properties of a reference model of seismic wave speed. In the ray approximation, Fermat's stationarity principle is invoked to replace the true ray path by the ray path in the reference model and changes of travel time as a result of event mislocation are approximated by a first order Taylor expansion of the travel time with respect to small changes in the source location (e.g. Spakman *et al.*, 1993). The quality of these approximations depends on the quality of the reference model in the sense of being already a close approximation of the seismic wave speed structure of the Earth. What close means in this respect has not been thoroughly investigated but experiments by van der Hilst and Spakman (1989) and Spakman *et al.* (1993) demonstrate that changing the reference model for mantle tomography significantly affects the tomographic model. This effect is also well known from local tomographic studies of the crust (e.g. Kissling *et al.*, 1994).
In global travel time tomography usually 1-D reference models are used in which wave speed only varies with depth. Different 1-D reference models exist (relating to different data types or subsets of global data) and several of these have been used as reference models in tomographic research as they already give a good approximation of the velocity distribution in the Earth. Nevertheless, lateral variations exist within the Earth being strongest in the crust and uppermost mantle. These 3-D heterogeneities obviously affect the travel times of waves and can also significantly modify the paths which rays take through the Earth (e.g. oceanic versus continental crust). Therefore, in many tomography studies corrections are applied to account for such 3-D structure. For example, in local teleseismic travel time tomography it has become standard procedure to correct travel times for crustal 3-D velocity structure beneath a seismometer array and afterwards fix crustal velocities in the inversion process (e.g. Sandoval *et al.*, 2003; Martin and Ritter, 2005). As another approach, heterogeneities in the crust can be included by forcing of the tomographic inverse model towards an assumed 3-D crustal model (Li *et al.*, 2006). This, however, neglects ray-bending effects.
By performing 3-D ray tracing, ray path geometry can be made consistent with 3-D structure obtained during inversion. This has been applied in various local and regional tomography studies (e.g. Papazachos and Nolet, 1997; Sandoval *et al.*, 2003) besides a few global nonlinear tomography studies (Bijwaard and Spakman, 2000; Widiyantoro *et al.*, 2000). So far, only Widiyantoro *et al.* (2000) have started directly from a 3-D reference model for their

tomographic inversions of 400,000 S-wave travel times.
In this study we will perform global tomographic experiments starting from different types of reference models (1-D and 3-D). Our aim is three-fold:

1. to investigate the dependence of global tomography models on the reference model used (1-D or 3-D reference models)
2. to create a tomographic model that combines the information contained in short period travel time data with that of long period seismic data
3. to relocate a large earthquake data set to account for the 3-D heterogeneities contained in the 3-D reference model

The scientific rationale underlying these three goals will be described in the following:

### 5.1.1 The dependence of global tomography on the reference model used

Even if a data set provides a perfectly resolved tomographic model, the linearizations and other theoretical simplifications made in the forward problem (e.g. adopting ray theory) may still produce spurious and biased results in the tomographic model. Data are back-projected along the wrong seismic ray paths (approximations of the real ray paths), and the seismic rays used generally start from the wrong source location. Effectively, these approximations cause inconsistency between the observations and forward model properties and translate implicitly into (correlated) data noise which may be mapped as spurious seismic wave speed anomalies or bias results both spatially and in imaged amplitudes (e.g. van der Hilst and Spakman, 1989; Spakman *et al.*, 1993). After a tomographic model has been obtained it can be used as a reference model for a subsequent forward modeling and inversion step in which 3-D ray tracing effectively provides linearization with respect to 3-D mantle structure imaged in the previous inversion step (Bijwaard and Spakman, 2000; Widiyantoro *et al.*, 2000). This may remove part of the bias but can only be expected to remove it completely if the ray set used provides near perfect spatial resolution. Yet, perfect resolution does not exist in global mantle tomography owing to the strongly non-uniform global distribution of earthquakes and seismological stations. As a result, (large) parts of the mantle are not well sampled leading to a poor resolution and a biased or spurious model. These parts of the model are mostly determined by the regularization used in the inverse problem. The regularization determines how properties of the reference model blend into the tomographic model. Rays that are traced through these parts of the model cannot converge to the real ray geometry and as a result the final tomographic model depends on the reference (starting) model. The only way to assess the dependence of the final model on the starting model is by experimenting with different starting models. In this study we present global tomography models based on 1-D and 3-D reference models, to assess the effects which different starting points may have on tomographic results.

### 5.1.2 Creating a tomographic model that combines the information contained in short period travel time data with that of long period seismic data

Depending on data type (short period travel time picks, long period travel times determined from waveform correlation, surface waves or normal modes), on tomographic technique (parameterization with spherical harmonic basis functions versus parameterization with local basis functions) and on regularization techniques (amplitude damping and/or derivative damping), distinctly different mantle models have been created although special regularization techniques can be used to improve similarity between models.
Models based on classical arrival time picks of short period P-waves and parameterized with local basis functions (e.g. conical cells) generally contain large, poorly resolved mantle volumes for which insufficient data exist to reliably image structure, for example, in the upper mantle below oceans, particularly in the southern hemisphere. When using the same data in conjunction with a parameterization with global basis functions (spherical harmonics) these data gaps are implicitly interpolated in the model space by virtue of the global nature of the basis functions. Boschi and Dziewonski (1999) offered reconciliation of both approaches by combining a cell parameterization with regularization based on first derivative damping. By its nature however, first derivative regularization interpolates (and extrapolates) in model space, particularly, in regions of few or no data constraints. These interpolated parts of the model remain, however, in the null space of the tomographic problem.
Tomography based on local parameterizations is particularly useful to exploit the resolving power of short period P-wave data in well sampled mantle regions (e.g. van der Hilst *et al.*, 1997; Bijwaard *et al.*, 1998) while tomography using global spherical harmonic basis functions is useful in conjunction with data with a relatively low sensitivity for the detail ($\lesssim 200$ km) of mantle structure such as normal modes, surface waves, and carefully selected long period S-wave or P-wave data (e.g. Li and Romanowicz, 1996; Ekström and Dziewonski, 1998; Ritsema *et al.*, 1999). Unlike travel time tomography models, such models are based on a more uniform sampling of mantle structure albeit at large wavelength (e.g. laterally 500-1000 km or larger). Long period data are largely complementary in sensitivity for mantle structure compared to the sensitivity of short period data, and in part complementary in spatial sampling of the mantle. A combined inversion of short period travel time data with long period data would be beneficial to arrive at a more complete structural model of the mantle.
In this study, we choose for a hybrid approach to reach this goal by taking independent (in data and technique) tomographic models based on long period data as reference models for tomographic inversion of short period P-wave data. In this way, the partly complementary structural information contained in long period data is already contained in the background of our experiments, and will (hopefully) be more focused in regions where the short period travel time data may prove to have superior resolving power for structural detail.

### 5.1.3 Nonlinear earthquake location in 3-D models of mantle structure

Standard, earthquakes are located in 1-D reference models (e.g. ISC, NEIC procedures). The procedure developed by Engdahl *et al.* (1998) particularly advocates the use of modern 1-D

reference models and empirical station corrections to, at least partially, account for effects of near-station crust and mantle structure. As noted earlier, tomographic models based on travel times (derived from earthquake location in 1-D models) show that large parts of the mantle are insufficiently resolved owing to lack of data. Travel time models based on local parameterization and using local regularization suggest that the resolving power of the short period P-wave data for the very long wavelength content of mantle structure may not be strong. Models constructed from long period data (including surface waves and normal modes) do, however, indicate the presence of very long wavelength mantle structure. One possibility for explaining this difference between models is that during earthquake location (part of) the signal belonging to long wavelength heterogeneity is mapped into a hypocenter mislocation depending on the global or regional station network involved for each event. A way around this potential problem is relocation of earthquakes in long wavelength tomography models. In this way, our procedure of using 3-D reference models requires 3-D location of the earthquakes prior to tomographic inversion in the 3-D reference model, which will also account for effects on the location of the far-field long wavelength structure of the mantle.

In summary, we anticipate that 3-D ray tracing and nonlinear earthquake location in a realistic 3-D reference model prior to tomographic inversion provide a better starting point for inversion than a simple 1-D reference model could. Independent of this, our hybrid approach of using long wavelength tomography models of Earth structure, which are constructed from long period data, as 3-D starting models for short-period travel time tomography will blend the structural information implicitly contained in short period data with that obtained from inversions of long period data. This leads to a more complete model than either approach by itself can deliver at present.

## 5.2 Data

### 5.2.1 EHB catalog

The main data source for travel time tomography is a reprocessed and updated version of the International Seismological Centre (ISC) bulletins extended with travel times from the National Earthquake Information Center (NEIC) of the U.S. Geological Survey for the most recent events (Engdahl *et al.*, 1998). This database will be referred to hereafter as EHB catalog. The latest version of this database contains earthquake observations for the period 1964–2004 including over 445,000 events for 27.4 mill. first and later arriving phases. The processing of Engdahl *et al.* (1998) comprised a phase re-identification, theoretical travel time calculation in the reference model ak135 (Kennett *et al.*, 1995) and source relocation involving corrections for crust and mantle heterogeneity. From that catalog, 7.9 mill. regional P arrivals, 9.7 mill. teleseismic P, pP and pwP arrivals and 1.5 mill. PcP, PKPab, PKPbc, PKPdf and PKiKP phases were selected for the global P tomography of this study. The selection criteria for epicentral distance and travel time residual range are given in Table 5.1. The precision of the P phases was estimated following the method of Gudmundsson *et al.* (1990). This method uses ray bundles of teleseismic phases with decreasing width to extrapolate the standard deviation of ray bundles with zero width, which is presumed to be the upper limit of

errors in the data. For the phases selected from the EHB catalog for $25° - 100°$ distance this error is estimated to be 0.65 s.

### 5.2.2 Euro-Mediterranean bulletin

The Euro-Mediterranean bulletin of the Euro-Mediterranean Seismological Centre (EMSC) provides the second data set used in this study. Like the EHB catalog, this bulletin contains a collection of travel time observations but only from local networks in the Euro-Mediterranean region (Godey *et al.*, 2006). Well constrained earthquakes in this catalog were relocated by the EMSC. However, if existent, the corresponding EHB location is used here instead of the EMSC locations. Otherwise, the events are relocated in ak135 including empirical regional travel time corrections for consistency with the EHB catalog following the approach of Engdahl *et al.* (1998) and using the relocation method described in Section 5.3. From the resulting EMSC subset, 155,000 travel time residuals from 14,000 events were selected using the selection criteria given in Table 5.1. Following the method of Gudmundsson *et al.* (1990), here the upper limit of random data errors was estimated to be 0.68 s.

### 5.2.3 Newly picked data for stations in Europe

Additionally, temporary experiments in Europe (CALIXTO (Wenzel *et al.*, 1998), EIFEL (Ritter *et al.*, 2000), MIDSEA (van der Lee *et al.*, 2001), SVEKALAPKO (Bock and the SVEKALAPKO Seismic Tomography Working Group, 2001), TOR (Gregersen *et al.*, 2002)), the ORFEUS archives (Observatories and Research Facilities for European Seismology) and a data collection from Leeds University, UK (Arrowsmith, 2003) form another source of data for travel time tomography. The data from these stations were obtained as waveforms, pre-processed and picked with the automatic picking method of Sandoval *et al.* (2004a). This procedure resulted in a total of 83,500 P-wave travel times (see also Chapter 4). The picking errors were estimated within the picking algorithm to be approximately 0.15 s. The obtained travel times were later on combined with the Euro-Mediterranean bulletin and EHB catalog data using the same selection criteria as for the EHB catalog.

### 5.2.4 Newly picked data for stations in North America

Furthermore, in North America many of the data registered and stored by the Advanced National Seismic Network (ANSS), the Incorporated Research Institutions for Seismology (IRIS), the Canadian National Seismic Network (CNSN), the Southern California Earthquake Data Center (SCEDC) and the NARS-Baja project (Trampert *et al.*, 2003) are not reported to the ISC on a regular basis. Data from these sources were obtained for 2002–2004 and build the fourth subset used here. Originally, the data set was acquired and picked by Sandoval *et al.* (2004a) as part of an investigation of the lithosphere and mantle beneath North America. It was obtained using the same processing as for the European data set and contains 120,000 P-wave picks for 486 events. As for the newly picked data for stations in Europe, the picking error is expected to be on the order of 0.15 s since they were obtained with the same picking method. Again, the same selection criteria as for the EHB catalog were applied.

| phase type | epicentral distance | residual range |
|---|---|---|
| P | $\leq 25^\circ$ | $\pm 7.5$ s |
| P | $> 25^\circ$ | $\pm 3.5$ s |
| pP, pwP (focal depth $\geq 35$ km) | $25^\circ - 100^\circ$ | $\pm 3.5$ s |
| PcP | $25^\circ - 40^\circ$, $47^\circ - 70^\circ$ | $\pm 3.5$ s |
| PKiKP, PKPdf | $110^\circ - 140^\circ$ | $\pm 3.5$ s |
| PKPab, PKPbc, PKPdf | $\geq 150^\circ$ | $\pm 3.5$ s |

**Table 5.1:** Selection criteria for the different phase types used for tomography.

## 5.3 Tomographic method

In seismic tomography, travel time residuals, i.e. the difference between observed arrival times and the corresponding reference model arrival times, are used to invert for 3-D velocity variations with respect to the reference model. In the high-frequency approximation, the Fresnel zone collapses into a seismic ray and seismic wave propagation theory reduces to seismic ray theory. In this approximation travel times are computed by integration of the slowness along the ray path resulting in the following delay time equation:

$$d = \underbrace{\int_L s \, dl}_{T_x(s)} - \underbrace{\int_{L_0} s_0 \, dl_0}_{T^0_{x_0}(s_0)} + \Delta t_x + \Delta t_s + \epsilon \tag{5.1}$$

where $d$ represents the delay/travel time residual, the first and second integral describe the computation of the "true" and predicted travel times $T_x(s)$ and $T^0_{x_0}(s_0)$ respectively with $L$ as ray path through the Earth starting at the true earthquake location $x$, $L_0$ as ray path in the reference model starting at the reference location $x_0$, $dl$ and $dl_0$ are the ray segments, $s$ is the Earth's slowness field and $s_0$ is the slowness field of the reference model. $\Delta t_x$ contains the timing error due to source mislocation as a result of the slowness anomaly field $s - s_0$, $\Delta t_s$ contains travel time effects due to station elevation and instrument response and $\epsilon$ describes the observational errors (e.g. picking errors or phase misidentification, remaining location errors). Equation 5.1 holds for any adopted reference model.
The first integral of equation 5.1 is linearized under the assumptions that the ray path in the reference model is sufficiently close to the actual ray path in the Earth ($L \approx L_0$) and that the reference earthquake locations are sufficiently close to the real locations. The effect of the spatial earthquake mislocation on the travel time is approximated by a Taylor expansion of the travel time around the reference source $x_0$. This leads to the forward equation of travel time tomography based on ray theory:

$$d = \int_{L_0} (s - s_0) \, dl_0 + (\mathbf{x} - \mathbf{x}_0) \cdot \nabla_0 T^0_{x_0} + \Delta t_x + \Delta t_s + \epsilon \tag{5.2}$$

In a tomographic analysis, a large set of delay time equations 5.2 derived from many source-station combinations is discretized and inverted for estimates of the slowness anomaly field

$s - s_0$, event mislocations $\mathbf{x} - \mathbf{x}_0$, origin time errors $\Delta t_x$ and the station statics term $\Delta t_s$. Following the approach of Bijwaard *et al.* (1998), composite rays are used instead of single rays for the EHB and EMSC data where a composite ray is built from single rays of the same phase type which are recorded at the same station and originate from the same event cluster (defined by volumes of $0.3^\circ \times 0.3^\circ \times dz$ with volume thickness $dz$ increasing from 15 km at the surface to 40 km at 660 km depth). In this way, the number of data for inversion is reduced and at the same time the signal-to-noise ratio increased. The data are weighted prior to inversion by the spread of the individual delay times within the respective ray bundle to account for the difference in ray bundle size.

$$W_{rb}^{-1} = \sqrt{\frac{\sum_{i=1}^{N} (\overline{dt} - dt_i)^2}{N}} \tag{5.3}$$

where $W_{rb}$ represents the ray bundle weight, $dt_i$ is the delay of ray $i$ and $\overline{dt}$ is the average delay of the ray bundle. The weights were restricted to one order of magnitude.
For the newly picked data (Section 5.2.3 and 5.2.4), this approach is not used as their quality is expected to be higher. Instead, single rays with large weight are used. The resulting data vector contains 10.4 million residuals from originally 19.4 million single residuals.
The Earth is parameterized by an irregular grid of non-overlapping cells according to the method of Spakman and Bijwaard (2001) where the cell size depends on the number of rays crossing a cell. The horizontal cell size varies in crust and mantle between 0.5°$\times$ 0.5° and 10.0°$\times$ 10.0° with an increasing layer thickness from the crust (10 km) to the lower mantle (200 km). The inner and outer core are both parameterized by a single layer with cells of 10°$\times$ 10° to allow for core structure but simultaneously prevent large model variations. The irregular grid is constructed from 8 035 000 cells of 0.5°$\times$ 0.5° which are projected using a hitcount constraint onto 604 000 non-overlapping irregular cells. The irregular cell approach mostly reduces overparameterization thereby improving the conditioning of the inversion matrix while retaining the possibility to resolve structure at small scales (0.5°) where allowed by the data.
The tomographic inversion itself is performed iteratively with the LSQR algorithm of Paige and Saunders (1982). Simultaneously with the inversion for cell slowness anomalies, we invert for event cluster mislocations and station corrections. A second-derivative damping is applied to regularize the solution of the inversion and to obtain a smooth model. Additionally, for inversion with 3-D reference models an amplitude damping is applied to suppress large model excursions particularly in the crust and directly beneath it. The model parameters are scaled for inversion dependent on cell size and hitcount to emphasize small cells and weigh down cells with very high hitcounts in the lower mantle following the approach of Bijwaard *et al.* (1998):

$$\begin{pmatrix} \mathbf{C}_d^{-1/2}\mathbf{A} \\ \lambda\mathbf{C} \end{pmatrix} \mathbf{S}^{-\frac{1}{2}}\mathbf{m}' = \begin{pmatrix} \mathbf{C}_d^{-1/2}\mathbf{d} \\ 0 \end{pmatrix} \tag{5.4}$$

where $\mathbf{A}$ contains the ray path segments, relocation and station coefficients, $\mathbf{C}_d$ represents the data covariance matrix, $\lambda$ is a damping factor controlling the trade-off between data misfit and model norm/smoothness varying between 1000 and 7000, $\mathbf{C}$ is the matrix of damping

coefficients, $\mathbf{S}$ the scaling matrix with $(S_{jj}) = h_j V_j$ and $h_j$ and $V_j$ are hitcount and cell volume respectively, $\mathbf{m}' = \mathbf{S}^{\frac{1}{2}}\mathbf{m}$ is the scaled model vector $\mathbf{m}$ and $\mathbf{d}$ the data vector consisting of the travel time residuals.

### 5.3.1 Reference Models

#### 1-D reference model

The radial model ak135 by Kennett *et al.* (1995), which has served as reference model in many other studies, is used as the 1-D reference model. The basic data set of travel time delays and earthquake locations is already consistent with this reference model. The tomographic model computed with respect to ak135 is hereafter called P06.

#### Long wavelength 3-D reference model

We constructed a 3-D reference model from two global tomography models determined from long period data. The CUB2.0 model (Ritzwoller *et al.*, 2002b) covers the crust and uppermost mantle and is combined with the model S20RTS (Ritsema *et al.*, 1999) in the deeper mantle. The CUB model is based on broadband surface wave group and phase velocity measurements and implicitly contains a global crustal model since it uses CRUST2.0 (Bassin *et al.*, 2000) in the background. The P velocities are taken as provided by this model. Between 200 and 300 km, the model S20RTS is smoothly blend in using a depth-weighted average of both models. S20RTS is based on Rayleigh wave phase velocity measurements, shear wave travel times and normal mode splitting measurements. Since S20RTS is a shear velocity model, it is converted to P velocities using the depth-dependent $d\ln v_s/d\ln v_p$ values of Bolton and Masters (2001) which range from 1.345 in the upper mantle to 3.45 in the lowermost mantle. In the Earth's core the 1-D reference model ak135 is used. The reference model is called CUB+S20RTS with which we compute two tomographic models: P06_CS obtained without a priori 3-D relocation of earthquakes, and P06_CSloc which is obtained starting from 3-D relocated events in the reference model CUB+S20RTS. Raypaths and travel time predictions in the reference models are obtained with 3-D raytracing (Bijwaard and Spakman, 1999a).

#### Hybrid 3-D reference model

It is well known that velocity anomaly amplitudes are systematically underestimated in travel time tomography as a result of reduced resolution, regularization, and incomplete convergence of the LSQR algorithm. Sensitivity tests with synthetic models demonstrate that in many regions recovered amplitudes are on the order of 50-70% of the synthetic amplitudes while the synthetic velocity patterns can still be well reconstructed. The amplitude loss cannot be recovered by inversion (it is in the null space) but amplitude enhancement can be made as part of the reference model. For this purpose (and for another reason discussed in section 5.5.3) a 3-D reference model is constructed that combines the better-resolved part of model P06 with reference model CUB+S20RTS. Prior to this combination the amplitudes of P06 are

first uniformly enhanced by a factor 2. Next, to correct for amplified amplitudes that would affect the data fit we only retain the part of the amplification that is located in the null space of the inverse problem. This part can be determined with the null space shuttle of Deal and Nolet (1996). The resulting model P06$^+$ is blended with reference model CUB+S20RTS leading to the new reference model CUB+S20RTS+P06$^+$. The reference model construction is implemented along the following lines: The tomographic inverse problem in which ak135 is used as reference model leads to the solution $\boldsymbol{x}_{P06}$ and is described by the following equation

$$\boldsymbol{A}\boldsymbol{x}_{P06} = \boldsymbol{d} \tag{5.5}$$

where $\boldsymbol{A}$ contains the ray path segments in each grid cell and $\boldsymbol{d}$ is the data vector. The difference between the amplified tomography model $\boldsymbol{x}_{amp}$ ($= 2\boldsymbol{x}_{P06}$) and the obtained model $\boldsymbol{x}_{P06}$ is

$$\boldsymbol{\Delta x} = \boldsymbol{x}_{amp} - \boldsymbol{x}_{P06} \tag{5.6}$$

The part of $\boldsymbol{\Delta x}$ which lies in the null space of $\boldsymbol{A}$ (i.e. $\boldsymbol{\Delta x}_{null}$) can be found by applying the null space shuttle of Deal and Nolet (1996): Let $\boldsymbol{h}$ be defined as

$$\boldsymbol{h} = \boldsymbol{A}\boldsymbol{\Delta x} \tag{5.7}$$

and $\boldsymbol{\Delta x}$ be the sum of the components lying in the range ($\boldsymbol{\Delta x}_{range}$) and in the null space ($\boldsymbol{\Delta x}_{null}$) of $\boldsymbol{A}$ such that

$$\boldsymbol{\Delta x} = \boldsymbol{\Delta x}_{range} + \boldsymbol{\Delta x}_{null} \tag{5.8}$$

Then inversion of

$$\boldsymbol{A}\boldsymbol{\Delta x} = \boldsymbol{A}(\boldsymbol{\Delta x}_{range} + \boldsymbol{\Delta x}_{null}) = \boldsymbol{h} \tag{5.9}$$

will give an estimate of $\boldsymbol{\Delta x}_{range}$ as $\boldsymbol{A}\boldsymbol{\Delta x}_{null} = \boldsymbol{0}$ by definition, so that the final amplified model (using eq. 5.8 to obtain $\boldsymbol{\Delta x_{null}}$)

$$\boldsymbol{x}_{P06^+} = \boldsymbol{x}_{P06} + \boldsymbol{\Delta x}_{null} \tag{5.10}$$

does not affect the data misfit since

$$\boldsymbol{A}\boldsymbol{x}_{P06^+} = \boldsymbol{A}\boldsymbol{x}_{P06} + \underbrace{\boldsymbol{A}\boldsymbol{\Delta x}_{null}}_{=0} = \boldsymbol{d} \tag{5.11}$$

The final, amplified model P06$^+$ is then combined with CUB+S20RTS applying a hitcount-dependent criterion where the hitcount is the number of rays crossing a cell. For cells with a hitcount greater than 500/1000/2000 in the upper/mid/lower mantle P06$^+$ is used. A gradual transition from P06$^+$ to CUB+S20RTS is achieved by using a hitcount-weighted average of both models in an intermediate hitcount range. For cells with a hitcount lower than 100/200/400 in the upper/mid/lower mantle CUB+S20RTS is used. Also, to ensure a smooth transition between P06 and CUB+S20RTS, the combined model is smoothed taking into account the adjacent cells in latitude and longitude direction. In the Earth's core the 1-D

reference model ak135 is used. With respect to reference model CUB+S20RTS+P06$^+$ we compute two tomographic models: P06_3D obtained without a priori 3-D relocation of earthquakes, and P06_3Dloc which is obtained starting from 3-D relocated events in the reference model CUB+S20RTS+P06$^+$. Again, raypaths and travel time predictions in the reference model are computed with 3-D raytracing.

### 5.3.2 Relocation

In the only other global tomography study using 3-D reference models of Widiyantoro *et al.* (2000), relocation of earthquakes in the actual reference model is neglected. Yet, to establish complete consistency between source parameters, travel times and the reference model, it is necessary to relocate the events in the 3-D reference models. The relocation procedure is based on the grid search method of Sambridge and Kennett (1986). Using the ak135 (EHB) location as starting point, the grid search is performed around this location. Initially, a grid of 2 km node spacing is used which is subsequently refined to 1 km node spacing. The grid nodes are supplied with theoretical travel times of the 3-D reference model using the ray tracing method of Bijwaard and Spakman (1999a).
From an analysis of the distributions of epicenter, depth and origin time shifts with respect to the original EHB locations, we discarded the 2% of relocations with the largest shifts in the tails of the respective distributions to avoid erroneous relocations. The rejected relocations consist mainly of events which are only regionally constrained or where only few arrival times could be used. Thus, for relocation in CUB+S20RTS 426,000 out of 450,000 earthquake relocations were accepted, for the rest we kept the original EHB location. For relocation with CUB+S20RTS+P06$^+$ 434,000 relocations were accepted. The differing numbers of accepted relocations and generally smaller relocation vectors for CUB+S20RTS+P06$^+$ indicate that CUB+S20RTS+P06$^+$ explains travel times better than CUB+S20RTS.

In summary, five tomographic models will be determined:

- P06 with respect to the 1-D reference model ak135
- P06_CS with respect to CUB+S20RTS but without 3-D relocation of events prior to inversion, i.e. 3-D ray tracing starts from ak135-locations
- P06_CSloc with respect to CUB+S20RTS with 3-D relocation in this reference model prior to inversion
- P06_3D with respect to CUB+S20RTS+P06$^+$ but without 3-D relocation of the events
- P06_3Dloc with respect to CUB+S20RTS+P06$^+$ and with 3-D relocation of the events prior to inversion

## 5.4 Model Resolution and Variance Estimates

Before analyzing and comparing the resulting tomography models, the spatial and amplitude errors of these models are estimated. As stations and events are not equally distributed over

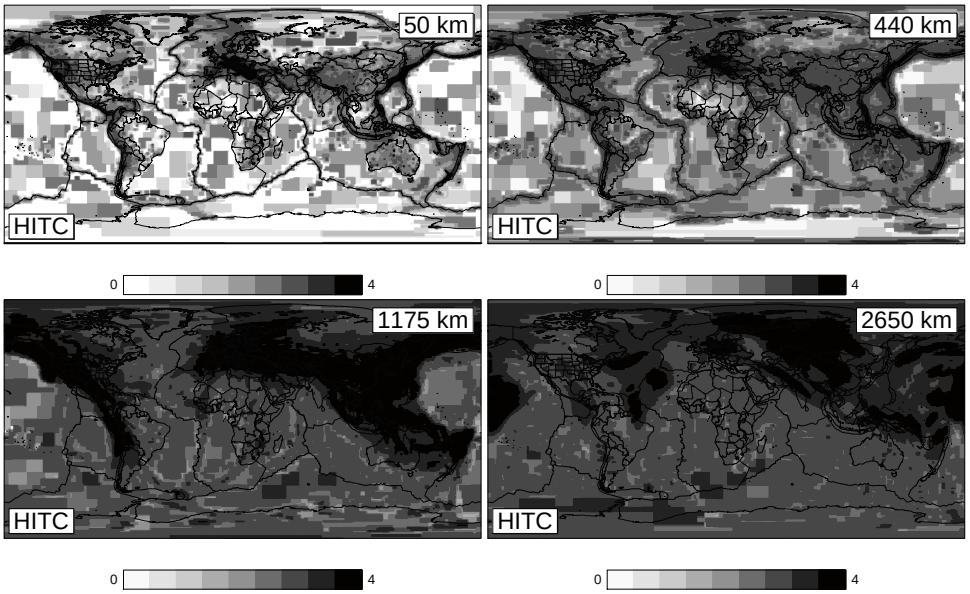


**Figure 5.1:** Logarithmic hitcount (i.e. number of rays crossing a cell) at 50 km, 440 km, 1175 km and 2650 km depths.

the Earth, the resolution of the velocity models varies spatially. The former fact is clearly indicated in the hitcount maps (Fig. 5.1). For example, ray coverage in the uppermost mantle is low beneath the oceans and cratons due to a low number of earthquakes and seismic stations.

The computation of the formal resolution matrix is practically excluded due to the large number of parameters, therefore tests are performed with synthetic models (Spakman and Nolet, 1988) to find the minimum size of anomalies that can be reconstructed and to detect lack of resolution. The synthetic models for these tests contain well separated spikes of $\pm 5\%$ amplitude with respect to the reference model with a distance of at least once the spike size in all directions between them and being shifted laterally with depth. The spike models are generated on an equal surface area grid and subsequently projected onto the irregular grid. Theoretical travel times are then calculated and Gaussian distributed noise with a standard deviation of $\pm 0.5$ s is added to the data. The spike amplitudes of $\pm 5\%$ are large compared to the overall seismic P-anomaly values typically imaged (few percent in the upper mantle, less than 1% in the lower mantle). We have adopted these synthetic amplitudes because they lead to a signal-to-noise ratio of the synthetic delays, which is comparable to that of the real data when Gaussian noise is added to the synthetic delays with a standard deviation of 0.5 s (comparable to data noise). We aim at a similar signal-to-noise-ratio because we want to mimic the inversion of real data as closely as possible. The reason why much larger synthetic amplitudes are needed to obtain a similar signal-to-noise ratio lies in the different structural character of real Earth structure and of the synthetic models used. Synthetic delays are acquired along rays that sample the alternating pattern of spike amplitudes where positive and negative contributions to the synthetic delay cancel for a large part along most ray paths. In

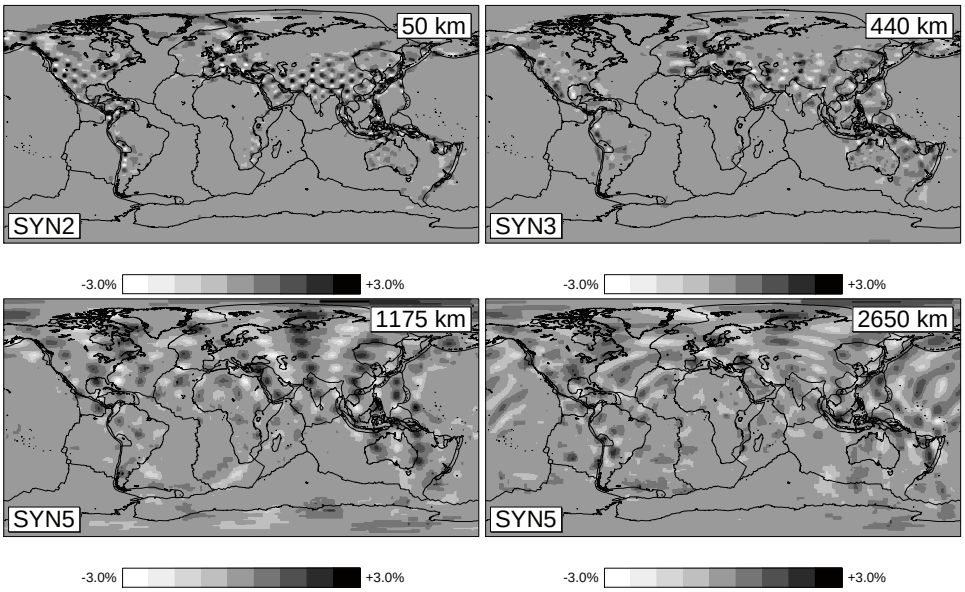


**Figure 5.2:** Spike tests for a cell size of 2°× 2° at 50 km depth, 3°× 3° at 440 km depth, 5°× 5° at 1175 km depth and 5°× 5° at 2650 km depth. The grayscales give the amplitude of the velocity anomalies.

this sense, the alternating spike model is typically a model that lies close to, and in practice usually partly in, the null space.

Earlier work (Bijwaard and Spakman, 2000) and our own experiments have shown that sensitivity test results, when using ray paths in a 1-D model or when using ray paths in 3-D models, only differ in small local detail which cannot be easily quantified as being a significant local improvement or degradation of spatial resolution. We are mainly interested in the more global effects of using different starting models for travel time tomography and have observed that the tomography models are not differently resolved on larger spatial scales, irrespective of the reference model used. For this reason we have concentrated on conducting sensitivity tests with the ray path set as computed in the 1-D ak135 reference model. The fact that spatial resolution on larger spatial scales is highly comparable between models renders resolution as less discriminative for comparison of results on global scales.

In Figure 5.2, 5.3 and the appendix of this thesis (Fig. A.1 to A.10), examples of such spike tests are shown at various depths with spikes of different sizes increasing with depth as the spatial resolution decreases with depth. While in the best resolved regions of the uppermost mantle anomalies of 0.5°×0.5° horizontally can be reconstructed, in the lowermost mantle only anomalies of 3.0°×3.0° to 4.0°×4.0° and bigger can be imaged (Figure 5.3). Furthermore, resolution is generally poor below oceans, in particular, in the southern hemisphere and in the lowermost mantle stronger lateral smearing is observed than at shallower depth.

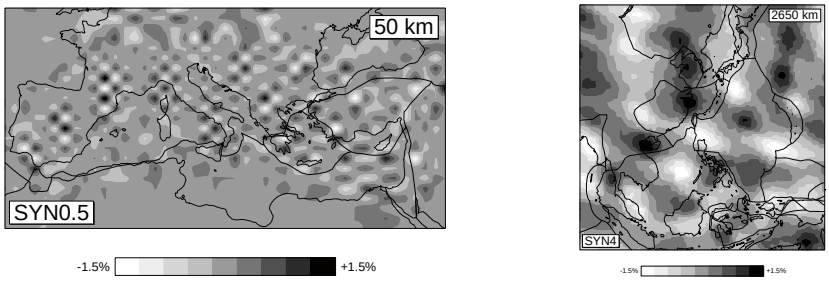


**Figure 5.3:** Blow-ups of spike tests for a cell size of 0.5°$\times$ 0.5° beneath Europe at 50 km depth and 4°$\times$ 4° beneath southeast Asia at 2650 km depth. The grayscales give the amplitude of the velocity anomalies.

To estimate the uncertainty of the velocity model caused by errors in the observed travel times, various methods can be applied, for example, using Gaussian distributed noise as data vector while keeping the original matrix for inversion (not performed here). As another test, the data vector can be permuted randomly before performing the inversion keeping again the same inversion matrix as for the original data vector (Spakman, 1991). This test also serves to investigate the correlation between data and ray paths where one would expect that the resulting model shows random anomalies of low amplitude if there are no correlations between delay times and ray paths. An example of such a test is given in Figure 5.4. In general, a random model with low amplitudes ($\approx 0.2 - 0.3\%$) is found in regions of good ray coverage. Only poorly sampled regions, as for example the Northern Atlantic at 50 km depth, display systematic anomalies of higher amplitude ($\approx 1\%$).

Data variance reduction obtained from the inversions ranges between 44.7% and 75.0% depending on how well the respective reference model already predicts the travel times (see Table 5.2). However, the inversions result in standard deviations of the weighted composite residuals between 1.44 to 1.58 for all models. The largest standard deviations are found for CUB+S20RTS as starting model while they are comparable for ak135 and CUB+S20RTS+P06$^+$ as starting models (taking into account that during 3-D ray tracing in the 3-D reference models noise on the order of 0.1 s is added to the residuals (Bijwaard and Spakman, 1999a)).

As a further analysis of model properties, the mean anomaly and the respective root-mean-square (RMS) values are computed for each layer and cells with a hitcount greater than 1000 (Fig. 5.5). The biggest model amplitudes are found in the crust and upper mantle. In particular, the models which implicitly contain CRUST2.0 display large average velocity perturbations in the crust with respect to ak135. On average, positive values are observed in the upper mantle in CUB+S20RTS and the according inversion models P06_CS and P06_CSloc as those models are dominated by high-velocity anomalies in regions sampled by short period P waves in the upper mantle while they are negative in the other models below 200 km depth. The mean values reduce to less than $\pm 0.2\%$ in the mid and lower mantle. For comparison, the mean velocity perturbations of the permuted data vector test are displayed which are close

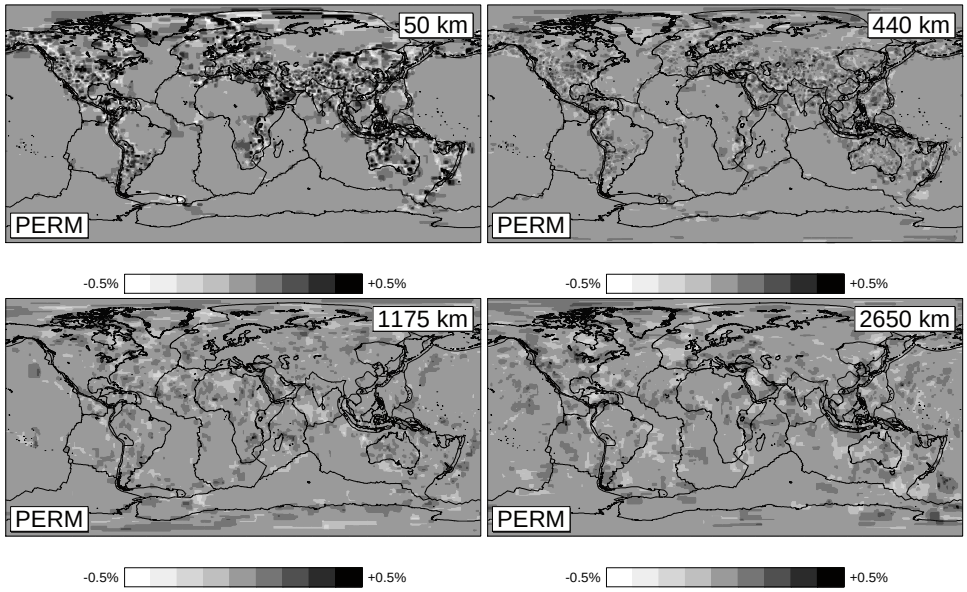


**Figure 5.4:** Sensitivity test with a randomly permuted data vector at 50 km, 440 km, 1175 km and 2650 km depth.

| | variance reduction from inversion | mean residual $\pm\sigma$ relative to the start. model before inversion | mean residual $\pm\sigma$ relative to the start. model after inversion |
|---|---|---|---|
| P06 | 52.1% | 0.07 $\pm$ 2.08 | 0.01$\pm$1.44 |
| P06_CSx | 75.0% | 1.30 $\pm$ 3.04 | 0.00$\pm$1.52 |
| P06_CSlocx | 61.6% | 0.11 $\pm$ 2.55 | 0.00$\pm$1.58 |
| P06_3Dx | 62.0% | -0.66 $\pm$ 2.40 | 0.00$\pm$1.48 |
| P06_3Dlocx | 44.7% | -0.14 $\pm$ 1.99 | 0.00$\pm$1.48 |

**Table 5.2:** Data variance reduction from inversion of all models and the mean $\pm$ standard deviation of the weighted composite residuals with respect to the starting model before and after inversion.

to 0% throughout the mantle.
High RMS values are found in the models with a 3-D reference model, in particular, for the inversion models P06_3D and P06_3Dloc. RMS values below the Moho reduce from ≈2.5% to 0.5%-0.7% at the 660 km discontinuity. In the mid and lower mantle, they are smaller with 0.1%-0.3% increasing again in the lowermost mantle. The model of the permuted data vector test contains RMS values of $\approx 0.25\%$ at the top, reducing to $\approx 0.2\%$ in the upper mantle and to $< 0.1\%$ in the lower mantle. This RMS profile resulting from the permuted data test provides an upper bound for the amplitude errors since the data are treated as errors in this test while true data errors are smaller.

## 5.5 Results

We focus on the tomographic models P06, P06_CSloc, and P06_3Dloc which are all obtained from inverting data sets (delays, ray paths, and hypocenters) that are consistent with the reference models used (ak135, CUB+S20RTS, and CUB+S20RTS+P06$^+$, respectively). For display and interpretation purposes all models are displayed with respect to reference model ak135. Using a different reference model for display than the starting model for inversion proves useful for interpretation of crust and mantle structures (e.g. Kissling and Spakman, 1996). Two other models are shown, P06_CSlocx and P06_3Dlocx, which constitute the actual inversion results with respect to the reference models CUB+S20RTS and CUB+S20RTS+P06$^+$, respectively, and show explicitly how and where the reference model is changed.

### 5.5.1 Tomography with respect to a 1-D reference model – P06

The first model (P06) will serve as a standard to which all other models will be compared to illustrate the effect of using a 3-D reference model. As the aim of this study is to investigate the dependence of global tomography on the reference model (e.g. relocation in the reference model, type of model used) we will present the main anomalies found in the tomography models only briefly. The information contained in the travel time residuals is easiest observed in the model P06 obtained with ak135 as reference model. In Figures 5.7 and 5.13, it is displayed in the top row at 50 km, 185 km, 440 km, 1175 km, 1900 km and 2650 km depth.
Interpretations can be given according to studies by Grand *et al.* (1997), Bijwaard *et al.* (1998), Bijwaard and Spakman (1999b), Goes *et al.* (1999), Rangin *et al.* (1999), van der Voo *et al.* (1999) and Montelli *et al.* (2006). In the upper mantle high-velocity anomalies are related to subducted slabs as, for example, along the Tonga-Kermadec trench (see also Fig. 5.8) or beneath southeast Asia (see also Fig. 5.9). Continental shields and cratons in the upper mantle are also imaged by high-velocity anomalies (e.g. the Canadian Shield or East European platform in Fig. 5.7 at 50 km, 185 km), while low-velocity anomalies are associated with tectonically active regions such as mountain ranges (e.g. Alps, North American Cordillera), back-arc basins (e.g. Western Mediterranean basin) or rifting/spreading centers (Mid-Atlantic ridge, Red Sea). Furthermore, low-velocity anomalies can be related to higher

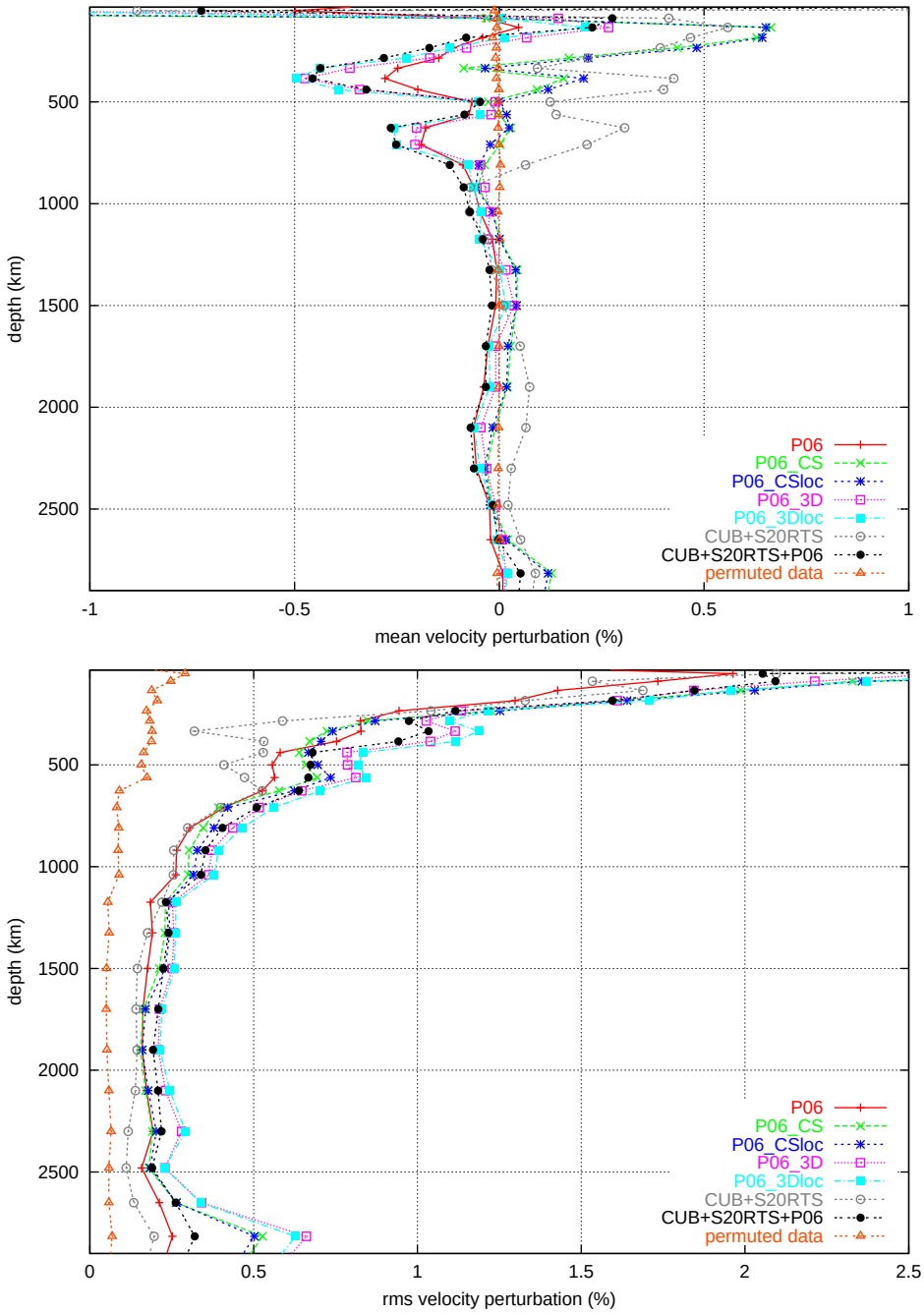


**Figure 5.5:** Depth-dependent laterally averaged velocity perturbation (top) and root-mean-square values (bottom) with respect to ak135 of the different models for regions sampled by more than 1000 rays.

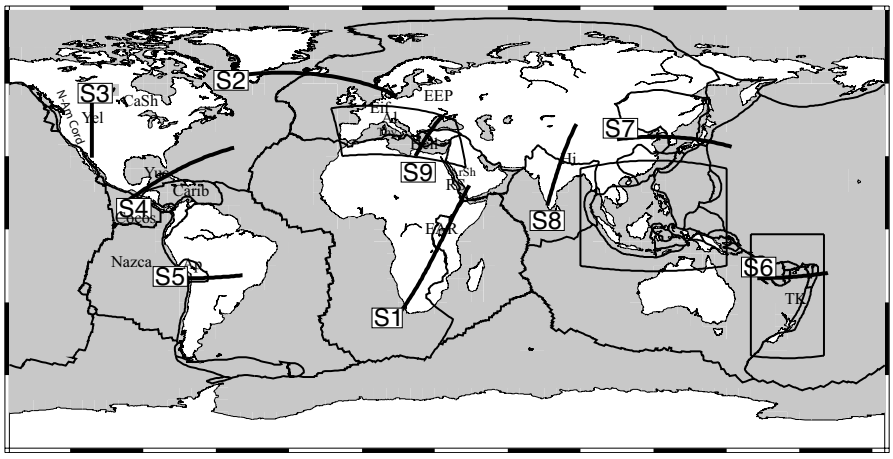


**Figure 5.6:** Location of the regions mentioned in the text, blow-ups (Figs. 5.8 to 5.10 and vertical cross-sections (Fig. 5.14). Abbreviations: Al - Alps, Ap - Altiplano, ArSh - Arabian Shield, CaSh - Canadian Shield, Carib - Caribbean plate, EAR - East African rift, EEP - East European platform, Eif - Eifel, Hi - Himalaya, N-Am Cord. - North American Cordillera, RS - Red Sea, Thy - Tyrrhenian Basin, TK - Tonga-Kermadec trench, Yel - Yellowstone, Yuc - Yucatan Basin. Plate boundaries after Bird (2003).

than average mantle temperatures in regions of presumed hot upwellings or plumes (e.g. Iceland, Eifel).
In the lower mantle, high-velocity anomalies represent remnants of subducted slabs as, for instance, at 1175 km depth the north-south oriented anomaly beneath the Americas related to the subduction of the Farallon plate or the west-east directed anomaly across Eurasia due to the subduction of the Tethys ocean. Low-velocity anomalies in the lower mantle, which are also observed at shallower depth, image plumes and hot upwellings as, for example, the low-velocity anomaly beneath the East African rift system or in Central Europe.
Besides that, undersampled regions can easily be detected in this model as they obtain $\pm 0\%$ velocity perturbations in the inversion.

### 5.5.2 Tomography with respect to the 3-D reference model CUB+S20RTS – model P06_CSloc

Figure 5.7 displays results for selected depths (figure columns) of models P06 (first row), P06_CSloc (second row), the actual inversion result P06_CSlocx (third row), and the reference model CUB+S20RTS (last row). The model P06_CSloc is the tomographic model obtained with CUB+S20RTS as starting model displayed with respect to ak135 and P06_CSlocx is the same model but displayed with respect to CUB+S20RTS.
In the crustal layers (not shown) only little information can be gained from the data except for a few regions in Europe, Japan or northwestern America where many stations and events exist. Therefore, in the crust the results are dominated by the reference model (CUB2.0 which

incorporates the crustal model CRUST2.0). Through event relocation and 3-D ray tracing in the reference model prior to inversion, ray path geometry and predicted travel times are still affected by the crustal heterogeneity (Bijwaard and Spakman, 1999a), which changes e.g. crustal entry/exit angles of rays and which has a global effect on ray geometry (i.e. with respect to rays in ak135).

At 50 km (Fig. 5.7) the resolving power of the travel time data set becomes apparent. At this depth, model resolution is mostly provided by uppermost mantle grazing Pn waves. P06_CSlocx (third row) shows explicitly where the reference model is changed. At 50 km, this solution mostly adds negative anomalies to the reference model, lowering the generally positive reference amplitudes found in many oceanic regions. Conversely, in the continental areas the solution tends to add small-amplitude positive anomalies to the reference model. Comparison to the P06 model explains that all these changes only occur where the travel time data indeed sample the uppermost mantle. Most of the oceanic areas and cores of continental regions retain reference model velocities for lack of ray sampling. Still, the inversion offers a good means to integrate seismic velocity information based on surface wave inversion (the reference model) with that obtained from travel time inversions.

A first glance at a depth of 185 km suggests great similarity between the reference model and P06_CSloc. On the global scale the changes are subtle but important as evidenced by the solution P06_CSlocx (third row) that, in many regions, shows narrow high-velocity variations and effectively adds the image of subducted slab to the reference model. This is even more convincing in cross-sectional view or mapview blow-ups (e.g. Figs 5.8, 5.9, 5.10, 5.14, discussed later). Apart from subduction zones, more complex variations in wave speed are required by the data in the European-Mediterranean region, the Tethys belt, southeast Asia and for instance under North America. For these regions and subduction zones the reference model is completely changed, attesting to the resolving power of the travel time data, and the model P06_CSloc resembles closely model P06.

Deeper in the mantle, where S20RTS provides the reference model, the amplitudes of the solution P06_CSlocx are more of the order of reference model wave speeds and the mantle volume sampled by seismic rays becomes much larger. Models P06 and P06_CSloc are quite similar in regions of good resolution. Differences between the two models occur mostly below oceanic areas where ray sampling is low and the data therefore have reduced resolving power to change the reference model. The depth-layer at 1175 km provides an illustration of these effects. Here, the 3-D reference model provides, although on a larger wavelength scale (smoother), a similar representation of the positive anomalies associated with subduction of the Tethys and Farallon oceans under Eurasia and the Americas, respectively. The solution P06_CSlocx looks rather random in structure but in fact focuses the reference model in these mantle subduction regions strongly towards P06 giving credit to the resolving power of the data set at this depth. Also below Africa, South America, and the north Atlantic, the reference model is strongly changed, focusing the "African super plume" (Ritsema *et al.*, 1999) in the former region, and focusing the "Iceland plume" (Bijwaard and Spakman, 1999b) in the latter.

Around all these regions a transition occurs toward reference model anomalies which are only exclusively found beneath the NE Pacific and SW Atlantic. Similar observations can be made for the layer at 1900 km where again the reference model is being focused toward

P06 and which demonstrates that the tomographic models P06 and P06_CSloc are relatively independent of the reference models in most regions.
Occasionally the inversion with respect to the 3-D reference model produces totally new anomalies that are neither found (or suggested) in P06 nor in the 3-D reference model. An example is the positive anomaly north of the Fiji region in the SW Pacific at a depth of 2650 km. This anomaly occurs in a region of moderate resolution. Other examples of strong focusing of barely visible, low-amplitude structures in P06 or in the reference model, are the positive anomalies in the Tonga region, in the Indian ocean, the SE Pacific, South America and the SW Atlantic region. Redistribution of teleseismic ray geometry in the 3-D model with respect to ak135 is largest in the deepest mantle and may lead to visibility and focusing of hitherto undiscovered structure.

### 5.5.3 Inversion with respect to the alternative 3-D reference model CUB+S20RTS+P06$^+$ – model P06_3Dloc

As the results have shown so far, in regions of good resolution (according to the sensitivity tests) the tomographic models are very similar independent of the reference model used. In regions of very low resolution the models mostly reflect the reference model. There is an intermediate range where the solution is reference model dependent due to the spatially variable but limited resolving power of the data. In these regions P06_CSloc is a mix between the 3-D reference model and model P06 and there is no obvious reason why one would prefer one specific solution. With the construction of reference model CUB+S20RTS+P06$^+$ we have chosen to replace the intermediate and well-resolved regions with P06$^+$, an amplitude-enhanced version of P06. With this choice we accept to bias the solution in these mantle volumes toward a solution based on ak135. By construction, P06$^+$ contains larger anomaly amplitudes than P06 due to model amplification in the null space but its features are generally similar in regions of good resolution. As P06$^+$ replaces CUB+S20RTS in regions sampled by most rays, we can also account better, through 3-D ray tracing, for the non-linearity of the inverse problem resulting from small-scale high-amplitude velocity heterogeneity (e.g. slabs). In Figures 5.11 and 5.12, two mapview sections are displayed showing the effect of anomaly amplification at 440 km depth under northwestern America and at 1900 km depth beneath southeast Asia. The part of the model amplification that lies in the null space is generally less than half the amplitude of P06.
Figure 5.13 displays the inversion results of model P06_3Dloc (in the same format as Figure 5.7). At first instance one might expect that the solution P06_3Dlocx would only give rise to moderate changes of the reference model because CUB+S20RTS+P06$^+$ already combines the best from inversion model P06 with reference model CUB+S20RTS. Furthermore, amplitude amplifications in P06$^+$ are retained to the null space, hence data insensitive. Instead, although less pronounced than in solution P06_CSlocx (Fig 5.7), we observe changes with substantial amplitude and spatial variation. The reason must be found in the fact that the null space shuttle experiment leading to P06$^+$ was performed with ak135 as a reference and that in less well-sampled regions CUB+S20RTS is employed. After construction of the reference model CUB+S20RTS+P06$^+$, all events have been relocated prior to inversion using 3-D ray

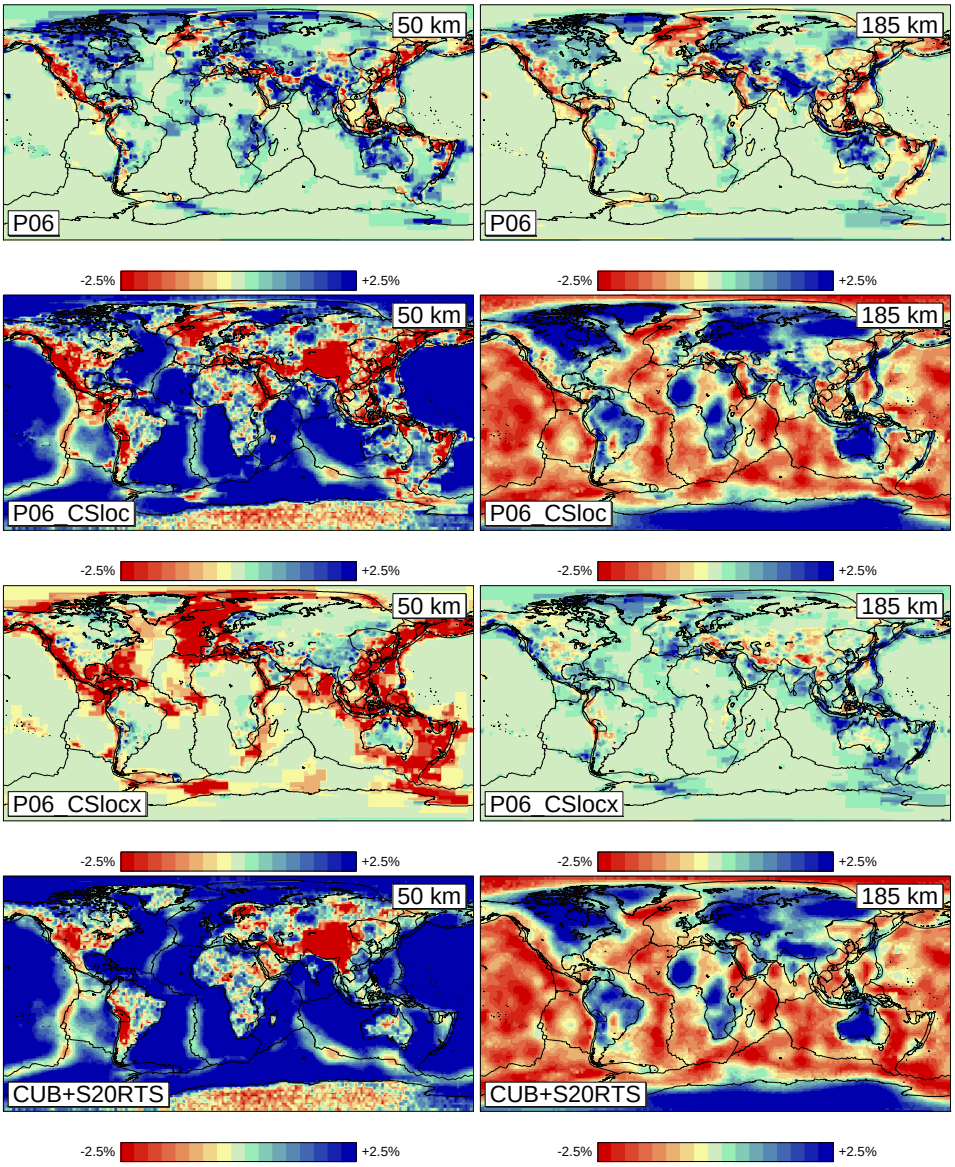


**Figure 5.7:** Tomography model P06 using ak135 as starting model (top), P06_CSloc using CUB+S20RTS as starting model displayed with respect to ak135 (second from top), P06_CSlocx using CUB+S20RTS as starting model displayed with respect to CUB+S20RTS (third from top) and the model CUB+S20RTS itself (bottom) displayed as velocity perturbations with respect to ak135. Shown are horizontal slices through the models at 50 km (left) and 185 km depth (right).

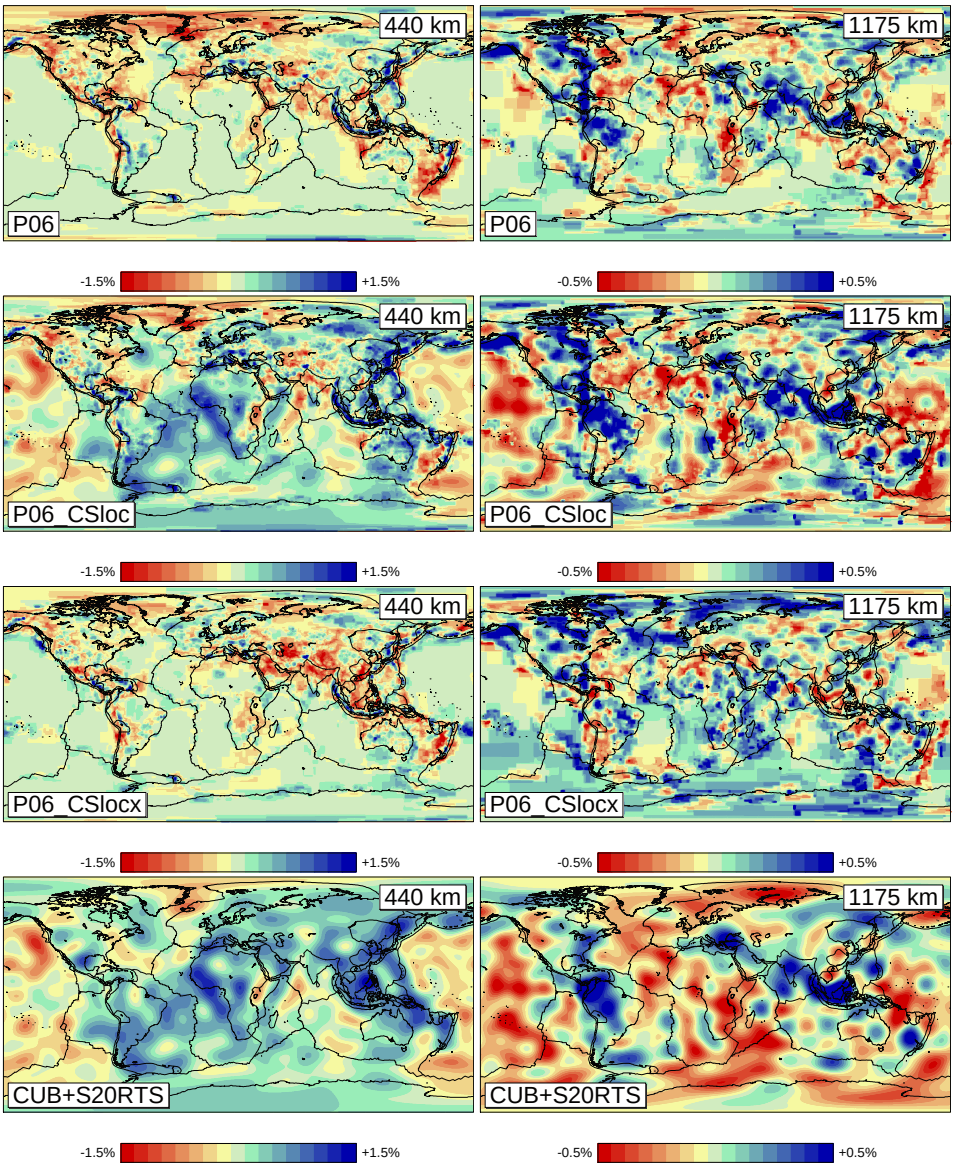


**Figure 5.7:** (Continued). Horizontal slices through the models at 440 km (left) and 1175 km depth (right).

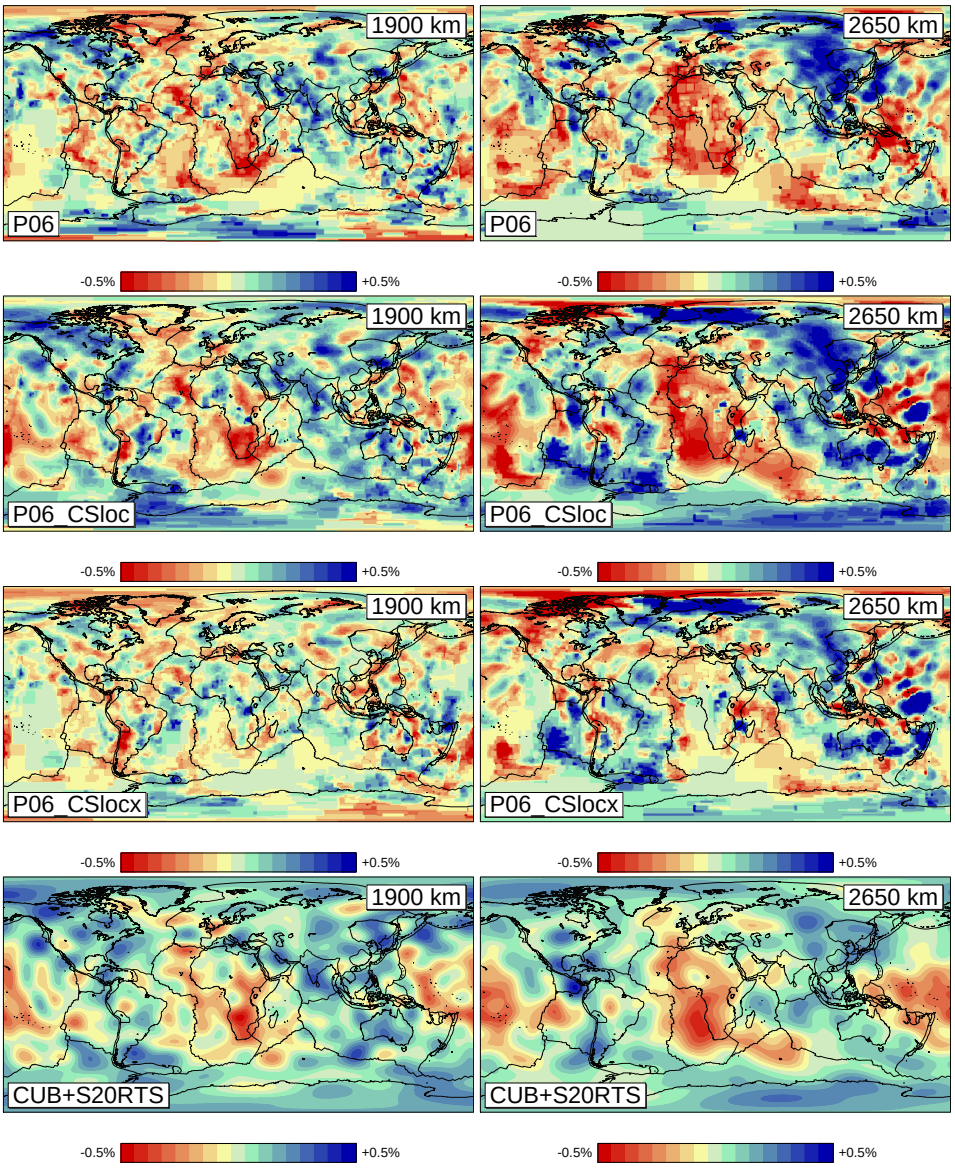


**Figure 5.7:** (Continued). Horizontal slices through the models at 1900 km (left) and 2650 km depths (right).

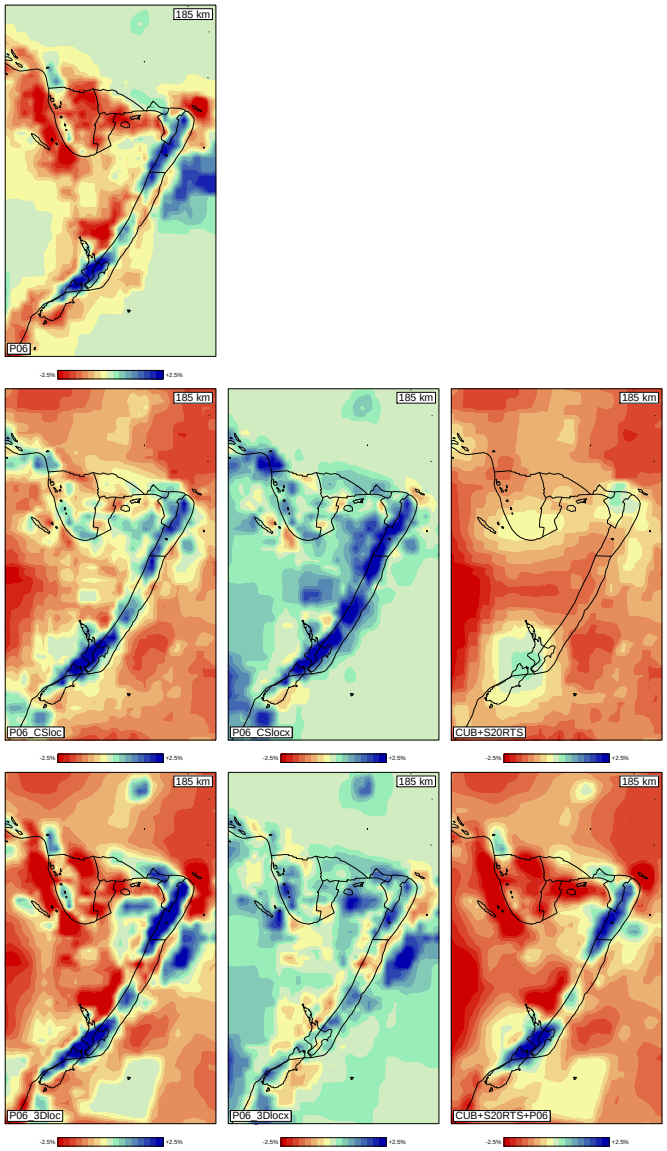


**Figure 5.8:** Model section at 185 km depth beneath the Tonga-Kermadec region. Tomography model P06 using ak135 as starting model (top), P06_CSloc using CUB+S20RTS as starting model displayed with respect to ak135 (middle row, left column), P06_CSlocx using CUB+S20RTS as starting model displayed with respect to CUB+S20RTS (middle column and row) and the model CUB+S20RTS itself (middle row, right column) displayed as velocity perturbation with respect to ak135. P06_3Dloc using CUB+S20RTS+P06$^+$ as starting model displayed with respect to ak135 (bottom row, left column), P06_3Dlocx using CUB+S20RTS+P06$^+$ as starting model displayed with respect to CUB+S20RTS+P06$^+$ (bottom row, middle column) and the model CUB+S20RTS+P06$^+$ itself (bottom row, right column) displayed as velocity perturbation with respect to ak135.

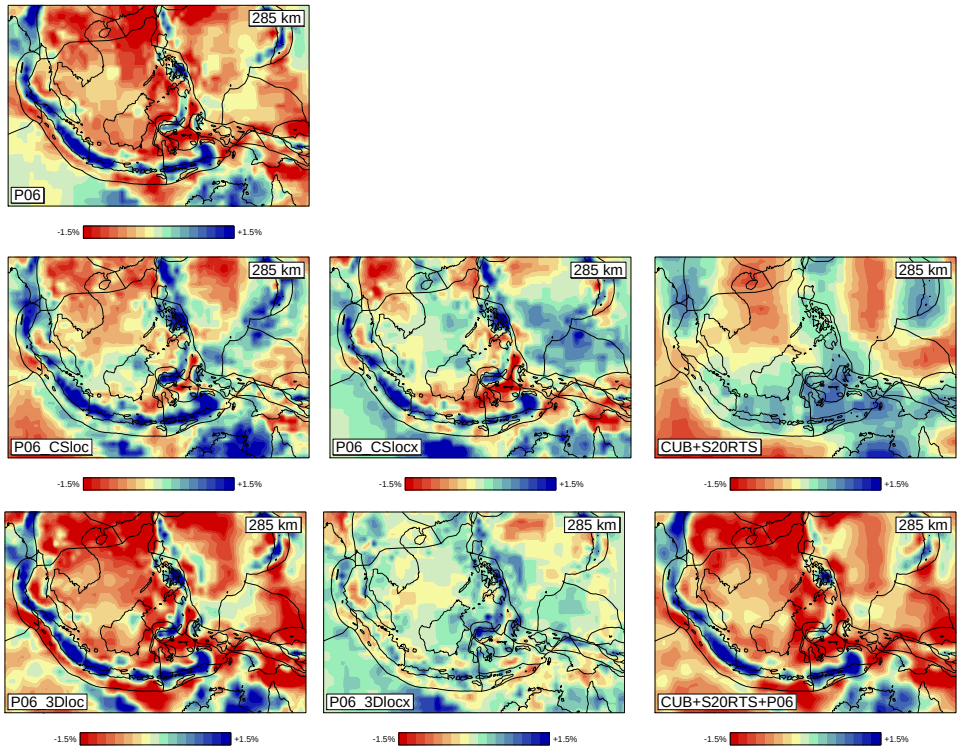


**Figure 5.9:** Model section at 285 km depth beneath southeast Asia. Models as in Figure 5.8.

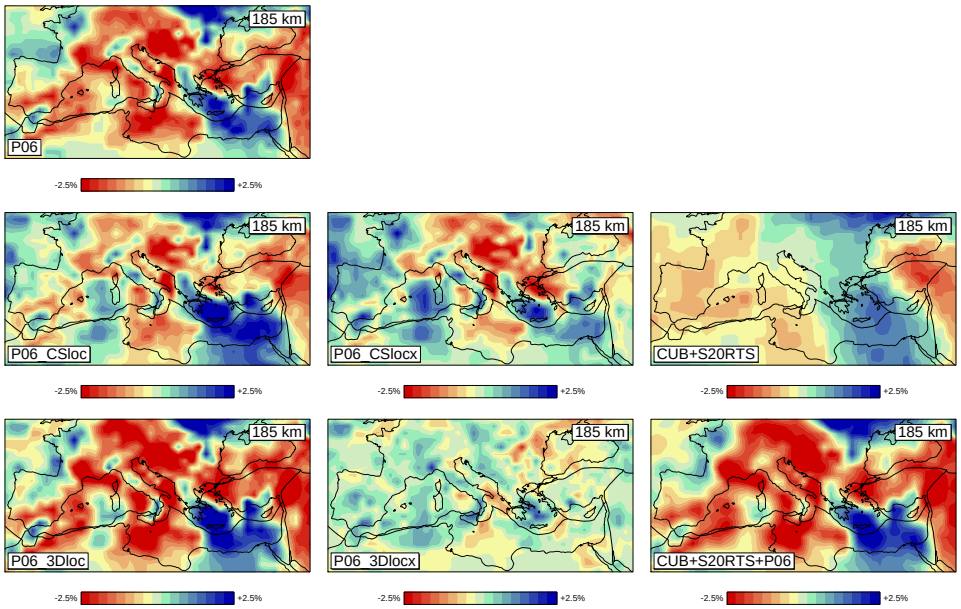


**Figure 5.10:** Model section at 185 km depth beneath the Europe-Mediterranean region. Models as in Figure 5.8.

tracing and leading to new delay times and 3-D ray paths. Hence, the amplitude amplifications are not necessarily completely lying in the null space of the current inverse problem and are subject to change. In contrast to ray tracing in reference model CUB+S20RTS, ray paths are now also traced through detailed 3-D heterogeneity, for example, in subduction regions which leads to focusing of slab structure and enhanced heterogeneity contrasts in model P06_3Dloc. These observations are similar to those of Bijwaard and Spakman (2000). Still, we should expect that the increased anomaly contrasts generally observed for P06_3Dloc compared to P06_CSloc are also partly contained in the null space as long as these are also present in the reference model.
At 50 km, P06_3Dlocx requires comparable corrections as P06_CSlocx which is understandable because in most of the affected regions the reference models CUB+S20RTS and CUB+S20RTS+P06$^+$ are the same. At 185 km of depth we notice a similar global effect but subtle differences exist which can only be observed in blow-ups of the models as given for some regions in Figures 5.8-5.10. These figures show invariably that, irrespective of already enhanced velocity contrasts between slab and ambient mantle contained in reference model CUB+S20RTS+P06$^+$, the inversion result P06_3Dlocx continuous to enhance these contrasts leading to even more focusing of structure as required by the travel time data. In the first part of the lower mantle, e.g. 1175 km depth, the correction P06_3Dlocx to the reference model tends to further focus the huge positive anomalies associated with Farallon and Tethys subduction and the low-velocity heterogeneity under eastern Africa. At 1900 km, the corrections are relatively smooth but do lead to enhancement of amplitudes and structure with respect to the reference model and also with respect to solution P06_CSloc. In the deepest mantle (2650 km), new structure is introduced under Europe and the Tonga-Fiji regions, while also under the Americas amplification of anomalies can be observed. At this depth, the difference in reference models in the lower hemisphere, where the resolving power of the data is relatively low, leads particularly to differences between the tomographic models P06_CSloc and P06_3Dloc.

### 5.5.4 Vertical cross sections

Differences and possible improvements of the presented inversion models can also be observed in vertical cross-sections (Figure 5.14), for which the locations are indicated in Figure 5.6. Starting with a section across East Africa (S1) where Ritsema *et al.* (1999) interpreted a hot upwelling in their model, we observe that this upwelling, being however narrower in mapview (see Fig. 5.7 and 5.13), is also retrieved with the travel time data.
While little velocity structure is imaged in S20RTS beneath Iceland (S2) in the mantle below 1800 km, all three travel time tomography models show low velocities originating at the base of the mantle as was imaged before by Bijwaard and Spakman (1999b).
It is still a question under debate if volcanism beneath Yellowstone is fed by a deep mantle plume and seismic tomography does not provide models yet which would allow a definite statement. However, independent of the applied reference model a low-velocity anomaly is imaged down to the core-mantle boundary to the south of Yellowstone (S3). It is most coherent in the upper 1400 km depth while between 1400 km and 1800 km depth a weak anomaly or respectively no anomaly at all is imaged.

Narrow outlines of the subducted Cocos plate beneath the Yucatan Basin (S4) are visible and the use of 3-D reference models increases the amplitudes of the tomography models below the 660 km discontinuity.
The subduction of the Nazca plate beneath South America (S5) looks similar in all travel time tomography models and shows that the subducted material accumulates in a vertical column in the lower mantle while S20RTS shows comparatively little detail in the lower mantle. The subduction zone in P06_CSloc is slightly broadened in the uppermost mantle while the data have enough resolving power otherwise to avoid overprinting by the reference model.
A cross-section of the Pacific plate subducting underneath the Australian plate at the Tonga trench (S6) shows for all tomography models the high-velocity structure of the subducted slab and in all sections it is visible that the slab penetrates the 660 km discontinuity. Again, the difference between the inversion models relates to the dependence on the reference model.
The subduction of the Pacific plate beneath Eurasia below Japan (S7) is very well resolved in all tomography models due to the large amount of data available.
The collision of the Indian plate with Eurasia (S8) displays many similarities in all tomography models despite the fact that CUB+S20RTS only shows one positive ”blob”, which again supports the reliability of the obtained models.
As a last example, the subduction of the African plate beneath Eurasia along the Hellenic arc is displayed (S9). Again, all three tomography models agree well with each other while CUB+S20RTS contains much less details. Evidently, the slab continues in all inversion models into the lower mantle.
In summary, these cross-sections demonstrate the resolving power of the travel time data set leading to imaging of comparable structures independent of the reference model.

### 5.5.5 Effects of relocation on tomography with 3-D reference models

Event relocation prior to tomography has several effects on tomography. When the EHB event location is used for computation of theoretical travel times in the 3-D reference models, baseline shifts occur as the mean velocity per layer of the 3-D reference models is not equal to ak135 at the according depth (see Fig 5.5). Relocation in the respective reference model removes this baseline shift of travel time residuals and reduces the scatter of the residuals (see Table 5.3, Figure 5.15). The residuals of the EHB catalog which originate from event location in model ak135 using regionalized heterogeneity corrections by Engdahl *et al.* (1998) show a narrow distribution centered around 0 s. In contrast, the residuals computed with respect to CUB+S20RTS for EHB locations exhibit a broader distribution due to the 3-D variations of the model and a baseline shift of 0.73 s appears as CUB+S20RTS is particularly in the upper mantle dominated by high-velocity anomalies (with respect to ak135). Relocating the events in CUB+S20RTS removes this baseline shift centering the residuals around 0.07 s and narrows the distribution. Also the travel time residuals computed for the final reference model CUB+S20RTS+P06$^+$ but starting from the EHB locations show a baseline shift although smaller (in absolute terms) than for CUB+S20RTS and negative (-0.36 s). Relocation centers the baseline shift around -0.04 s and the scatter in the residuals is even smaller than for ak135 indicating a better travel time prediction. Consequently, to establish consistency between source parameters and travel time residuals, a relocation is mandatory.

| | mean residual (s) | standard deviation (s) |
|---|---|---|
| AK135 (EHB) | -0.01 | 1.37 |
| CUB+S20RTS | 0.73 | 1.87 |
| CUB+S20RTS,loc | 0.07 | 1.66 |
| CUB+S20RTS+P06$^+$ | -0.36 | 1.49 |
| CUB+S20RTS+P06$^+$,loc | -0.04 | 1.28 |

**Table 5.3:** The mean $\pm$ standard deviations of the unweighted, single travel time residuals computed for the different reference models without and with earthquake relocation in the respective reference model (see also Fig. 5.15).

Other observations concern the tomographic inversion for velocity perturbations and simultaneous inversion for event cluster relocations and station corrections.
The difference between the models with and without a priori relocation shows that the largest changes appear in the crust and the uppermost mantle where most earthquakes are located. In particular in subduction zones, velocities increase when a relocation is performed beforehand resulting in more focussed slab anomalies (see, for example, the Sunda subduction zone at 90 km depth in Fig. 5.16). Deeper in the mantle, differences are less systematic but still velocity contrasts such as below Australia (Fig. 5.17) at 1175 km depth are enhanced. In the lowermost mantle, only few changes are observed.
Station corrections, which are obtained as part of the inversion, correlate well with average station residuals before inversion. Furthermore, the corrections are regionally systematic. Thus, they mainly serve to remove average station delays, most likely related to the (crustal) velocity structure beneath the stations not accounted for by the reference and tomography models. Relocation prior to inversion results in particular for the model CUB+S20RTS in smaller station corrections indicating that the inconsistency between travel times and source parameters without a priori relocation is partially compensated by increased station corrections.
Also, simultaneously with the inversion for 3-D velocity variations, event cluster relocation terms are obtained for the composite residuals. However, they are of limited value since they were determined without S and sP phases and represent entire clusters of earthquakes. The direction of the relocation vectors is regionally systematic and depending on the used reference model with a trade-off between hypocenter depth and origin time corrections as observed in previous studies (e.g. Bijwaard *et al.*, 1998).

## 5.6 Discussion and Conclusions

We have conducted mantle tomography experiments with 1-D and 3-D reference models inverting a very large data set of P-wave travel times. Using distinctly different reference models implies inverting distinctly different delay time data sets, as reference model predictions of travel times are different. Reference model independent wave speed structure could be retrieved for large mantle regions where, according to sensitivity tests, spatial resolution is good to moderate. In other regions mantle structure inverted from the travel time information

blended with the reference model velocities or the reference model was found unchanged.
The first 3-D reference model was composed from CUB2.0 in the crust and uppermost mantle overlying S20RTS in the deeper mantle. Interestingly, after 3-D location of all events in the reference model it proved that travel time predictions are worse than in the 1-D model ak135 (Table 5.3). This is surprising since both CUB2.0 and S20RTS are tomographic models derived from long period data and are assumed to give a better representation of mantle structure than a simple 1-D model. Improved locations combined with improved mantle structure should basically lead to a better travel time prediction (smaller delay times). We have not yet traced the reasons for this. Possible reasons can be that: (1) the locations in ak135 were performed using station corrections related to station elevation, crust and mantle heterogeneity (Engdahl *et al.*, 1998) while we did not use that in our location procedure, (2) the long wavelength models image different seismic velocities or have stronger amplitudes than in the real mantle as a result of insufficient damping during inversion (high-variance models), (3) the conversion between P and S velocity anomalies with the scaling factors of Bolton and Masters (2001) is not appropriate at all depths or more likely (4) the long wavelength models lack short wavelength structures (e.g. subducted slabs) which significantly affect travel times.

The best performing reference model in terms of travel time prediction is CUB+S20RTS+P06$^+$ although the difference with ak135 is small. Travel time predictions in the resulting inversion model P06_3Dloc (see Chapter 8) also demonstrates that this model predicts travel times better than ak135. Irrespective of the different statistics of the input data for inversion, still highly comparable models could be found with acceptable normalized data misfit (Table 5.2). The additional data error resulting from 3-D ray tracing, which we estimate to be of the order of 0.1 s, presumably slightly increases the misfit relative to that achieved in the P06 inversion and also increases the standard deviation prior to inversion.
Basically we have obtained the following results:

1. A new tomographic model P06 is computed relative to reference model ak135 and based on much more data than before.
2. Using an internally consistent procedure involving 3-D ray tracing, 3-D earthquake relocation and tomographic inversion, we have combined mantle structure obtained from short period travel time inversion with the structure imaged in long wavelength tomography based on long period data. This leads to two totally new mantle models, P06_CSloc and P06_3Dloc, of which we prefer the latter because it includes travel time and ray geometrical effects associated with strong amplitude and short-wave length heterogeneity (e.g. slabs) in the well resolved part of the mantle. P06_3Dloc also predicts travel times better than ak135.
3. We have demonstrated that short period P-wave delay times contain sufficient resolving power to completely replace, in well resolved mantle volumes, the high-amplitude long wavelength structure as obtained by inversion of long period data. A similar observation was made by Widiyantoro *et al.* (2000) from their inversions of S-wave travel times.
4. By using different reference models as starting point for inversion we have shown that, in the well-resolved mantle volumes, imaged structure is independent of the reference

model used which supports the actual existence of imaged structure.

5. Reference model dependence of inversion results occurs in regions where tomographic models (considerably) disagree and model quality thus depends on the quality of the reference model.
6. With relocation prior to tomography using a 3-D reference model, generally velocity contrasts across subduction zones are enhanced allowing for a better separation of effects of source location from velocity heterogeneities.

Apart from regional details, all models have comparable spatial resolution as they are basically obtained from the same data set and, on a global scale, fairly similar ray geometry. Discrimination between these models should be made on account of the quality of travel time data prediction. The statistical significance of usually small changes in data fit relies on precise knowledge of data errors which is unfortunately mostly absent for the huge data set of mostly hand-picked data.
The models P06_CSloc and P06_3Dloc can serve as global reference models for earthquake location and waveform modeling, as back ground models for regional tomography, as starting models for global travel time or waveform tomography, as background for regional seismotectonic studies, or may prove useful in studies of mantle dynamics and the gravity field of the Earth.
Overall, our preferred model is the model P06_3Dloc as it shows low data misfits comparable to P06 after inversion (see Tbl. 5.2), was obtained with raytracing in a detailed 3-D reference model and furthermore implicitly contains realistic lateral velocity anomalies in regions that are not well sampled by short period P waves.

## 5.7 Acknowledgments

We thank the ISC, NEIC, ANSS, ORFEUS, CNSN, IRIS, SCEDC, Stephen Arrowsmith, the CALIXTO, EIFEL, MIDSEA, NARS-Baja, SVEKALAPKO and TOR working groups for providing the data used in this study and M. Ritzwoller and J. Ritsema for providing the 3-D reference models used in this study. Computational resources for this work were provided by the EUROMARGINS programme of the European Science Foundation (01-LEC-MA22F WESTMED) and by the Netherlands Research Center for Integrated Solid Earth Science (ISES 3.2.5 High End Scientific Computation Resources).

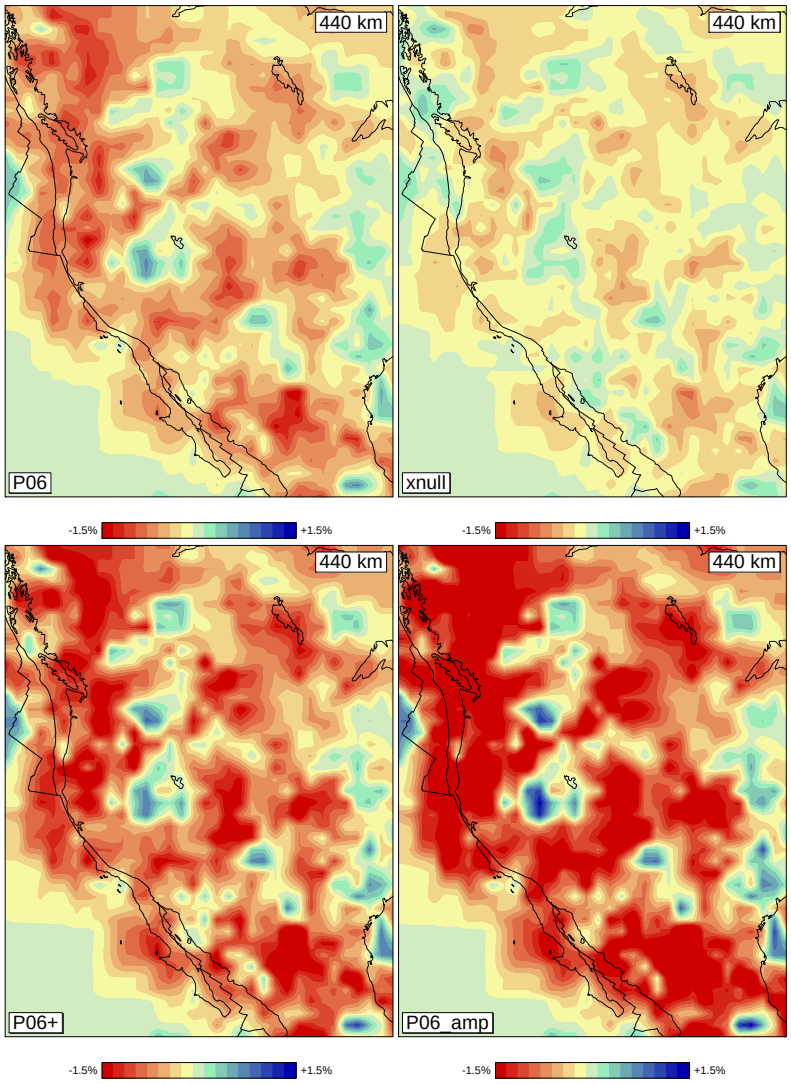


**Figure 5.11:** Model section at 440 km depth beneath western North America. Tomography model P06 using ak135 as starting model (top, left), xnull (top, right) is the model part $\boldsymbol{\Delta x}_{null}$ of the amplification that lies in the null space of $\mathbf{A}$, P06$^+$ (bottom, left) is the model P06+$\boldsymbol{\Delta x}_{null}$ and P06_amp (bottom, right) is the model P06 amplified by a factor of 2.

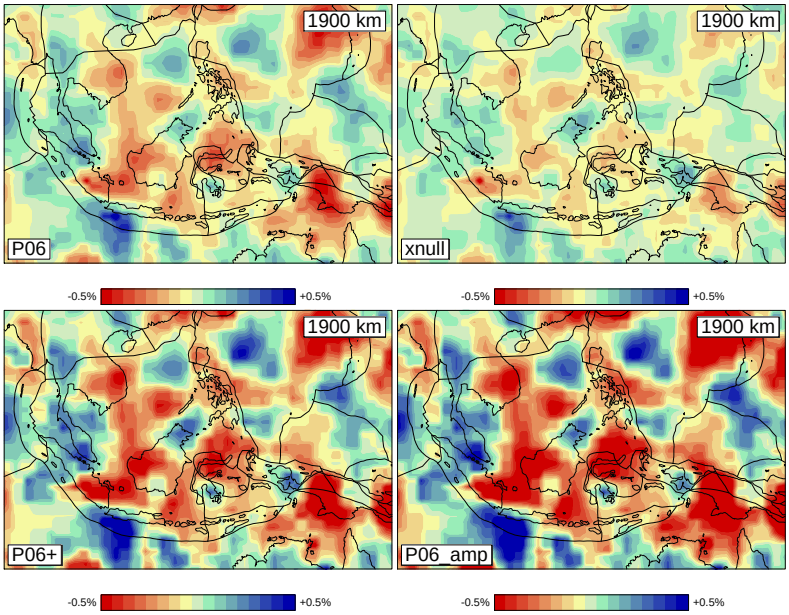


**Figure 5.12:** Model section at 1900 km depth beneath southeast Asia. Tomography model P06 using ak135 as starting model (top, left), xnull (top, right) is the model part $\boldsymbol{\Delta x}_{null}$ of the amplification that lies in the null space of $\mathbf{A}$, P06$^{+}$ (bottom, left) is the model P06 $+\boldsymbol{\Delta x}_{null}$ and P06_amp (bottom, right) is the model P06 amplified by a factor of 2.

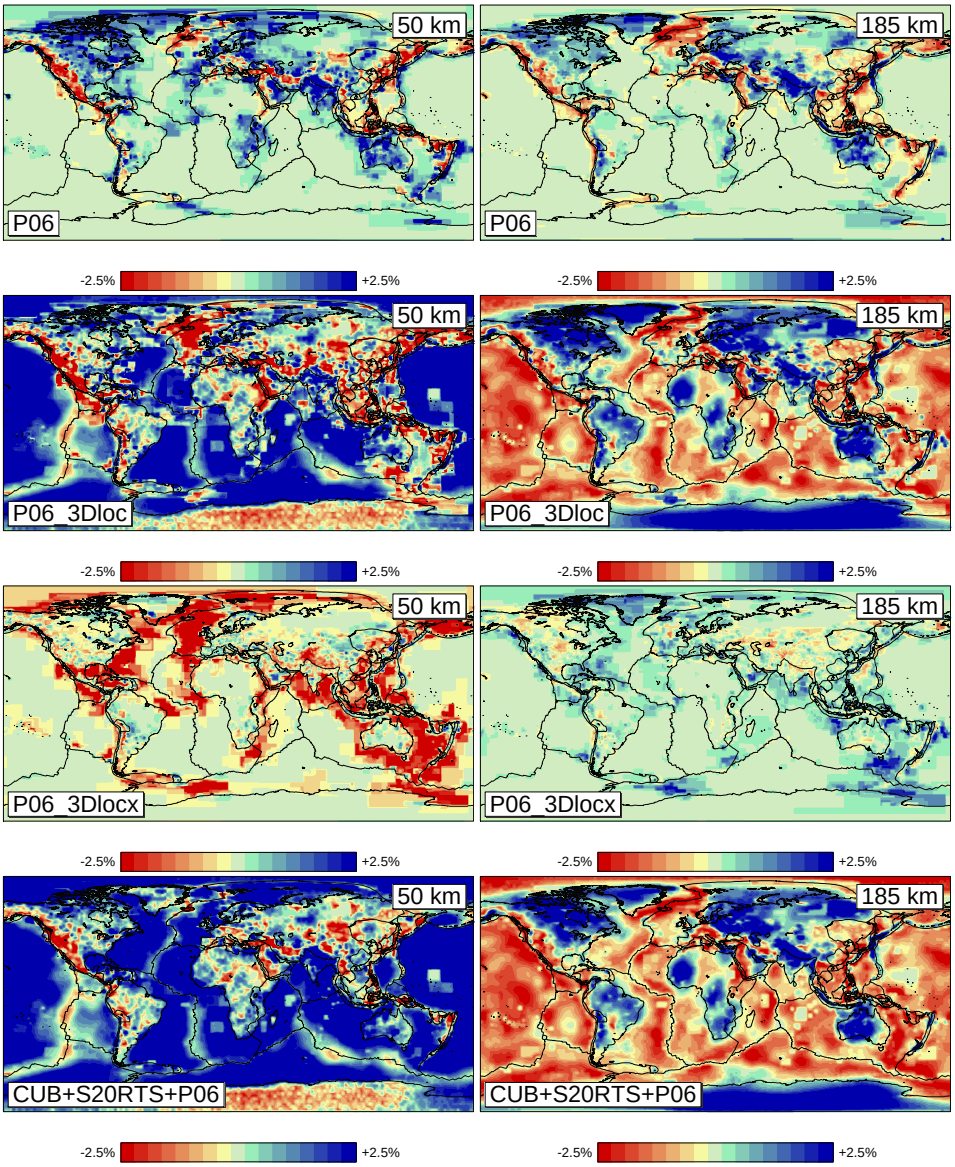


**Figure 5.13:** Tomography model P06 using ak135 as starting model (top), P06_3Dloc using CUB+S20RTS+P06$^+$ as starting model displayed with respect to ak135 (second from top), P06_3Dlocx using CUB+S20RTS+P06$^+$ as starting model displayed with respect to CUB+S20RTS+P06$^+$ (third from top) and the model CUB+S20RTS+P06$^+$ itself (bottom) displayed as velocity perturbations with respect to ak135. Shown are horizontal slices through the models at 50 km (left) and 185 km depth (right).

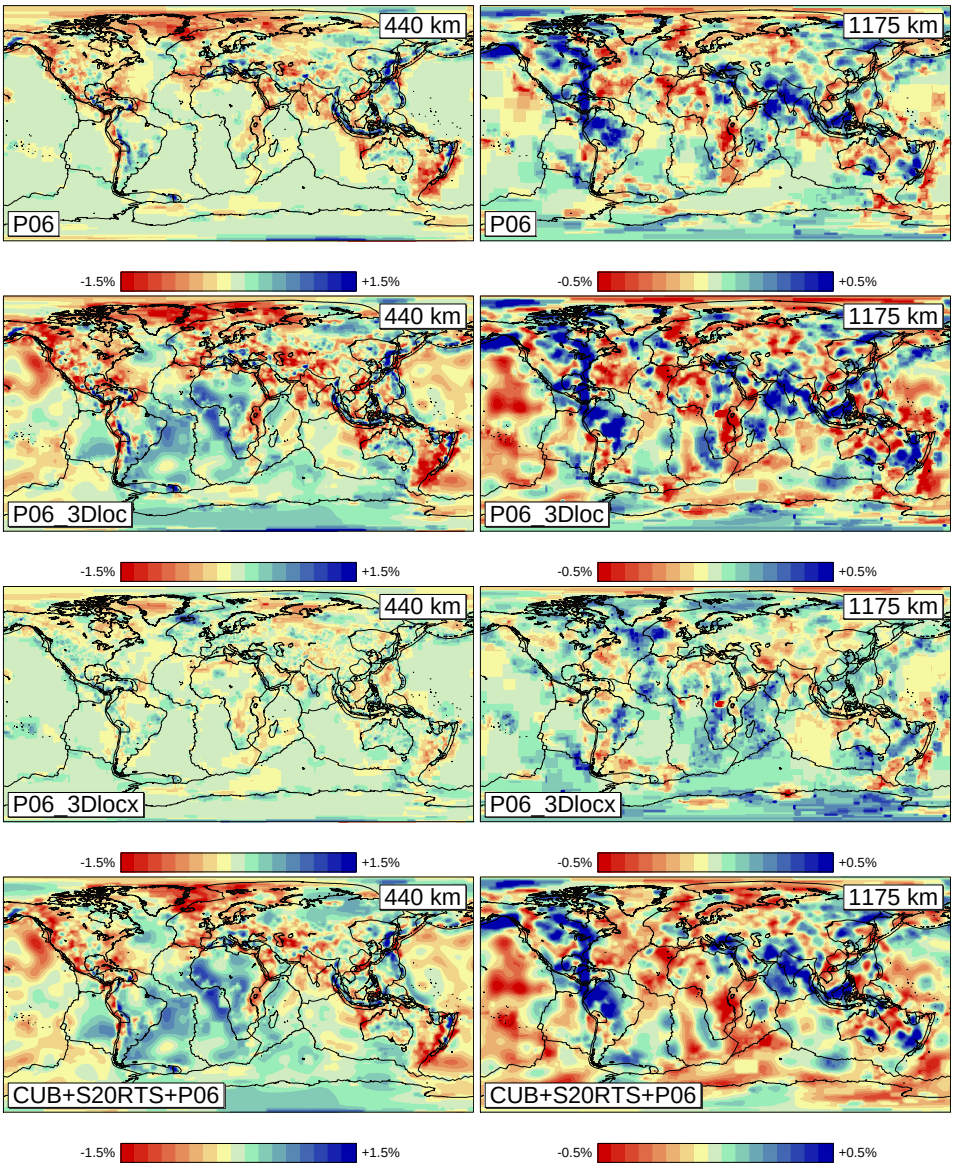


**Figure 5.13:** (Continued). Horizontal slices through the models at 440 km (left) and 1175 km depth (right).

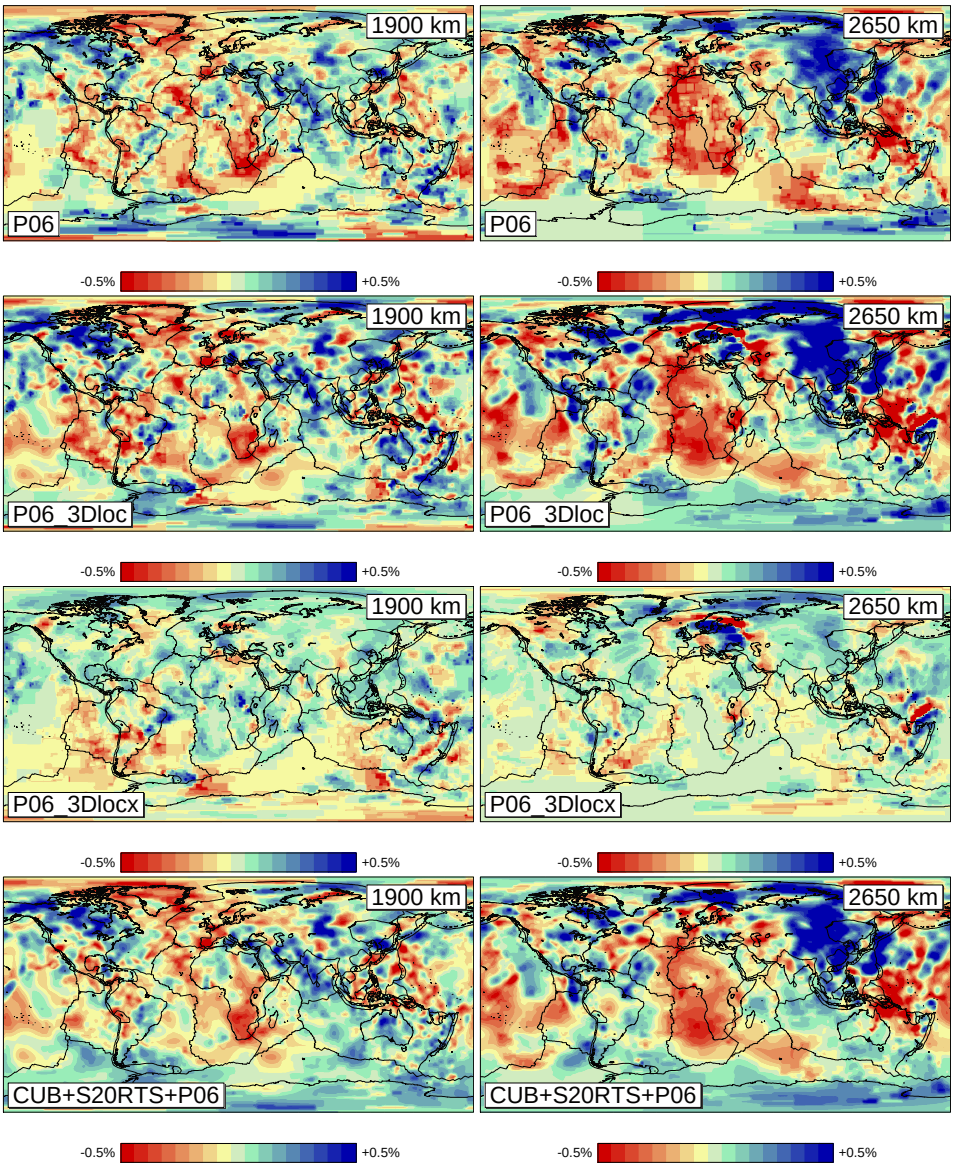


**Figure 5.13:** (Continued). Horizontal slices through the models at 1900 km (left) and 2650 km depth (right).

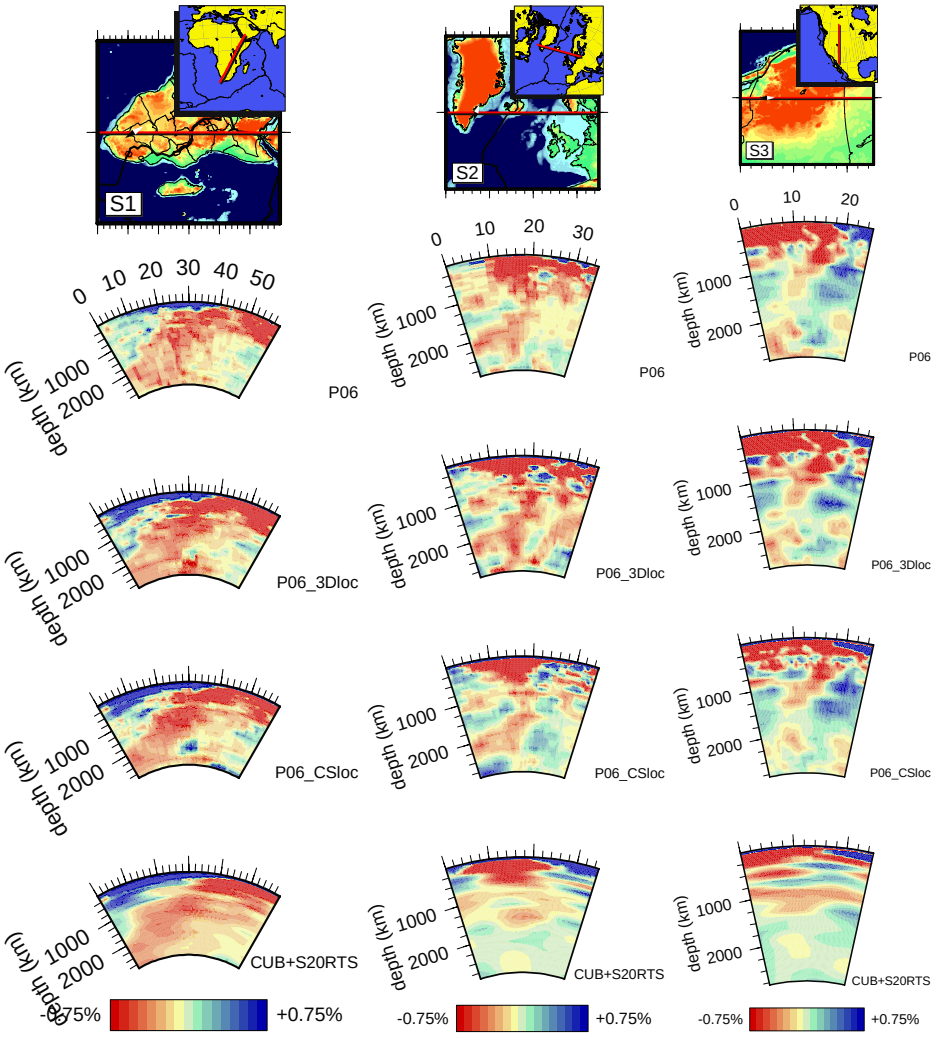


**Figure 5.14:** Vertical cross-sections displayed with respect to ak135 through the tomography models below East Africa (S1), Iceland (S2) and Northwest America (S3) for the tomography models using ak135 (top), CUB+S20RTS+P06$^{+}$ (second from top), CUB+S02RTS (third from top) as reference model and the reference model CUB+S20RTS itself (bottom).

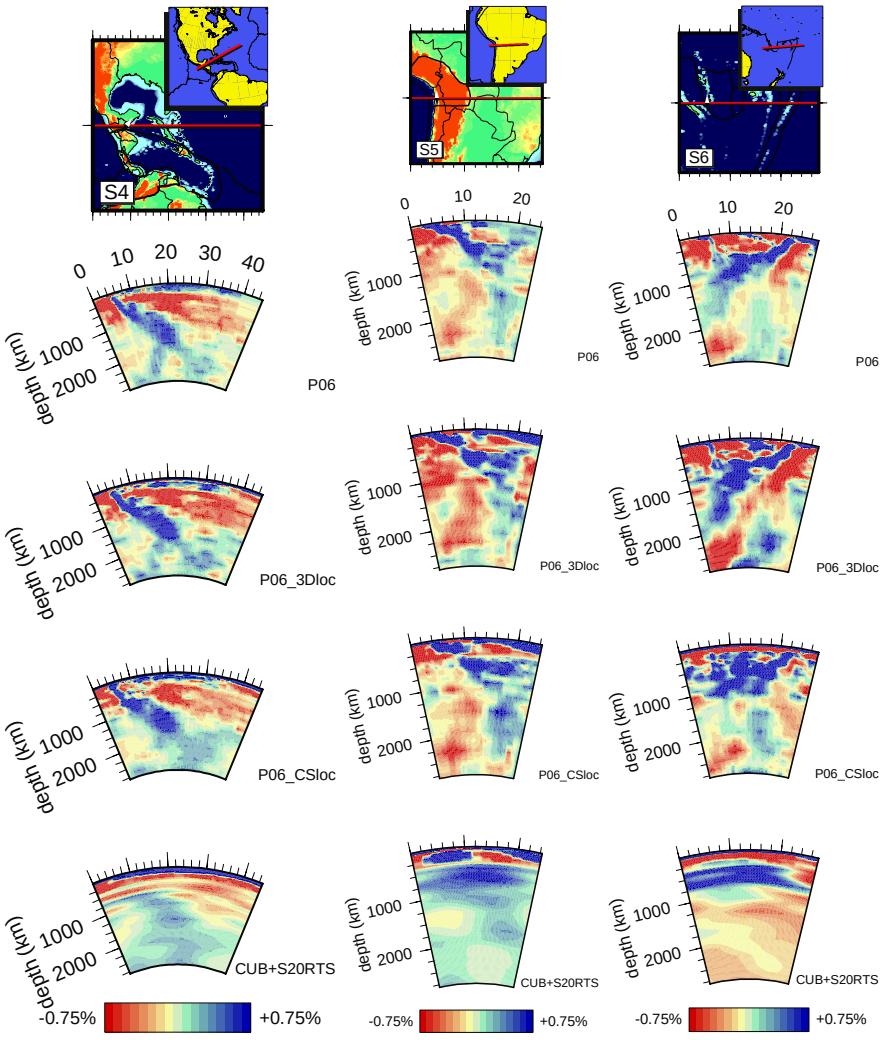


**Figure 5.14:** (Continued). Vertical cross-sections through the tomography models below the Carribean plate (S4), the Altiplano plate (S5) and Tonga (S6).

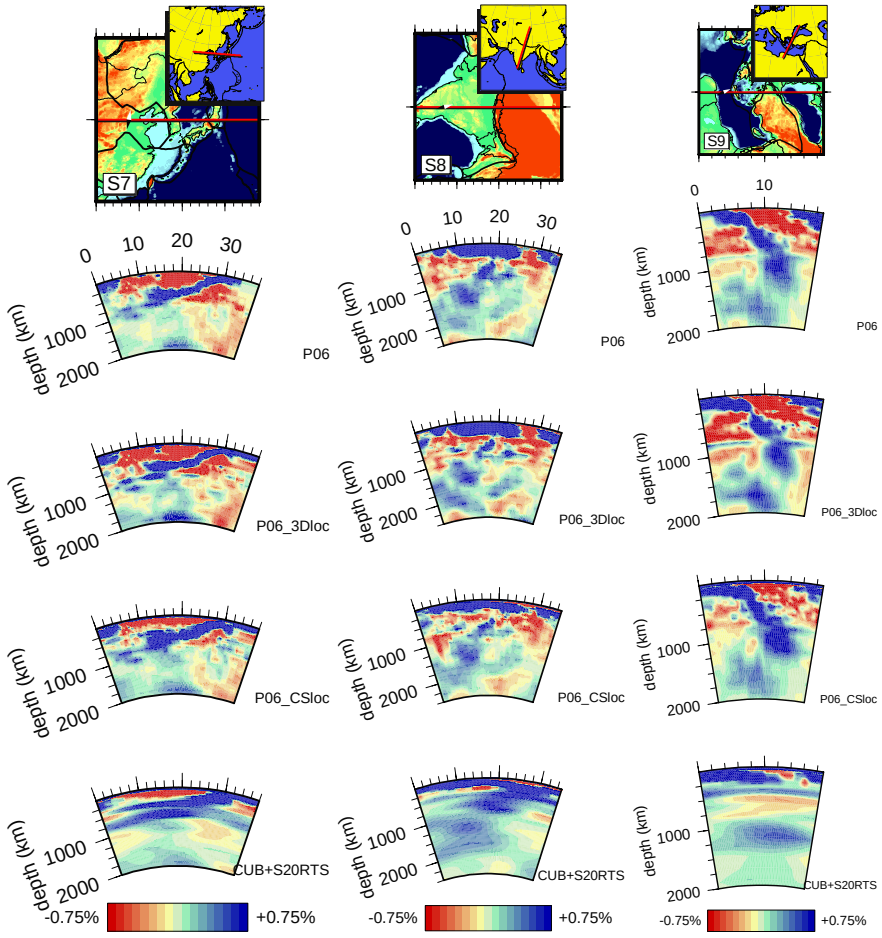


**Figure 5.14:** (Continued). Vertical cross-sections through the tomography models below Japan (S7), across the Himalaya (S8) and the Hellenic Arc (S9).

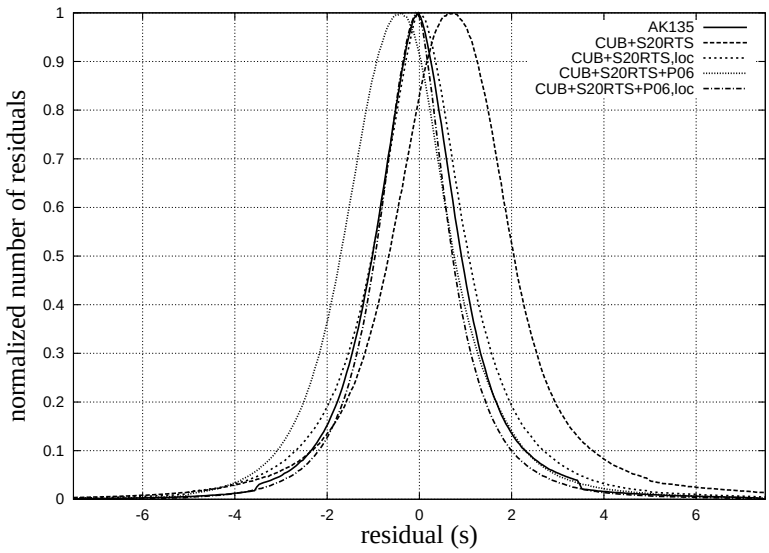


**Figure 5.15:** Histogram of the travel time residuals normalized to the maximum number versus the residuals computed with respect to AK135, CUB+S20RTS with/without a priori relocation and CUB+S20RTS+P06$^{+}$ with/without a priori relocation.

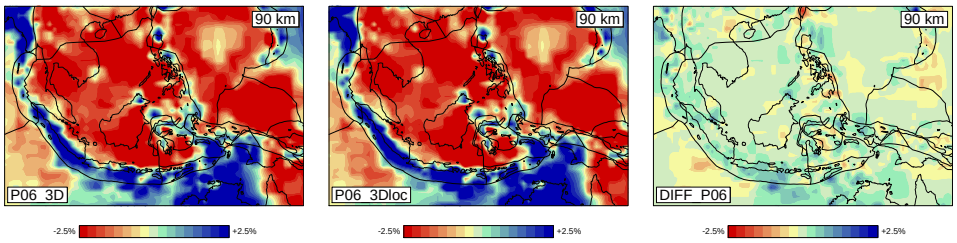


**Figure 5.16:** Section at 90 km depth beneath southeast Asia of the model P06_3D (without relocation prior to inversion), the model P06_3Dloc (with prior relocation) and their difference DIFF_P06. Blue are areas in DIFF_P06 where the model with a priori relocation contains higher velocities than the model without relocation and red are the regions where it is slower.

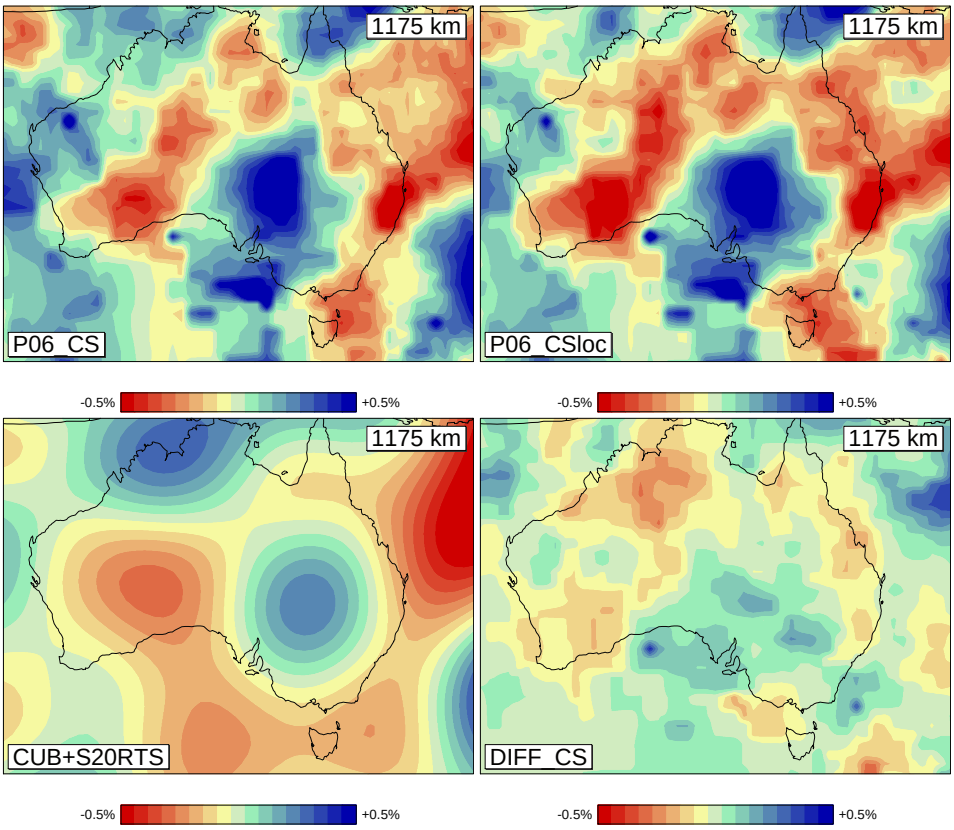


**Figure 5.17:** Section at 1175 km depth beneath Australia of the model P06_CS (without relocation prior to inversion), the model P06_CSloc (with prior relocation), the according starting model CUB+S20RTS and the difference DIFF_CS between P06_CS and P06_CSloc. Blue are areas in DIFF_CS where the model with a priori relocation contains higher velocities than the model without relocation and red are the regions where it is slower.

# Chapter 6

# Enhanced models of the European crust and mantle derived from travel time tomography

Seismic tomography has provided detailed images of the crust and mantle beneath Europe at both local and continental scale. The aim of this study is to improve imaging of the European mantle by combining arrival times from the International Seismological Centre (ISC) with additional arrival times from temporary experiments, data archives and bulletins incorporating also phase types which were not used before. As tomographic method, a regularized least squares inversion is performed for global mantle structure using an irregular grid parameterization. The inversions are performed both with a 1-D and a 3-D reference/starting model where the latter requires relocation of all earthquakes and 3-D ray tracing prior to the tomographic inversion. For the Europe-Mediterranean region, synthetic tests show that anomalies up to $0.5^\circ \times 0.5^\circ$ can be reconstructed in the best sampled regions of the uppermost mantle with resolution decreasing with depth. The added data sets are inverted separately to verify their quality showing that the obtained models contain velocity information also observed in other studies. The inversion results using the entire data set provide detailed velocity models of the mantle beneath Europe. Comparison with a previous model applying the same method shows that the new models image much more detail and enhance anomaly contrasts.

## 6.1 Introduction

The seismic velocity structure of the Europe-Mediterranean mantle has been subject of many tomographic studies both on local and regional scale (see Spakman and Wortel (2004) or Piromallo and Morelli (2003) for an overview).
Many of the global and regional high-frequency travel time tomography studies are primarily based on data from the International Seismological Centre (ISC) bulletins which provide the largest data collection available and is still expanding. For Europe, additional data are